REACTOR PHYSICS ANALYSIS OF AIR-COOLED NUCLEAR

SYSTEM

A Thesis

by

HANNIEL JOUVAIN HONANG

Submitted to the Office of Graduate and Professional Studies of
Texas A&M University
in partial fulfillment of the requirements for the degree of

MASTER OF SCIENCE

Chair of Committee,	Pavel V. Tsvetkov
Committee Members,	Marc Holtzapple
	Sean McDeavitt
Head of Department,	Yassin Hassan

May 2016

Major Subject: Nuclear Engineering

ABSTRACT

The design of SACRé (Small Air-Cooled Reactor) fixated on evaluations of air as a potential coolant. The assessment offered in this thesis focused on reactor physic analyses, and materials review and incorporation in a system defined by a highly corrosive environment. The oxidizing nature of air at high-temperature warrants the need to examine and compare materials for their oxidation temperature, their melting and boiling temperature, and their thermal conductivity. Material choices for the fuel, the cladding, the system's casing/structural material and the reflector were evaluated in this study.

Survey of materials and literature lead to the selection of six different cladding materials which are FeCrAl, APMT, Inconel 718 and stainless steel of type 304, 316 and 310. A review of their thermal properties, for a high oxidation temperature and melting temperature and the exhibition of a hard neutron spectrum lead to the selection of APMT steel material. This material was not only be selected as the fuel cladding but also as a casing for reflector and shielding materials.

The design of this 600 MWth system was investigated considering reflector materials for fast spectrum. Lead-based reflectors (lead bismuth eutectic, lead oxide and pure lead), magnesium-based reflectors (magnesium oxide and magnesium aluminum oxide), and aluminum oxide reflectors were evaluated in this thesis. The design configurations were compared to determine those which provide a hard neutron spectrum, an economically appropriate cycle length, a low breeding ratio and the least amount of neutrons escaping the reactor. The assessments of these notable characteristics lead to the selection of MgO reflector. This reflector allowed the system to operate for six years, for a corresponding burnup of 85 MWd/kgU.

The thermal setting of 875°C fuel temperature and 575°C of coolant and structural temperature promoted the design of a system with a fuel volume fraction smaller than that of the coolant volume fraction (40.28% - 45.01% respectively). This configuration was promoted favorable over an active core with a fuel volume fraction higher than or equal to the coolant volume fraction because of some thermal properties of air like a small thermal conductivity, specific heat and density.

ACKNOWLEDGEMENTS

NOMENCLATURE

<u>Abbreviation</u>

ASU	Air Separation Unit
BOC	Beginning of Cycle
DLOCA	Depressurization Loss Of Coolant
DOE	Department of Energy
EOC	End of Cycle
Fa	Fuel Assemblies
GFR	Gas Fast Reactor
HLW	High Level Waste
K_{eff}	Criticality Constant
LFR	Lead Fast Reactor
LWR	Light Water Reactor
MCNP	Monte Carlo N-Particle
MTL	MATLAB
Nbr	Number
ODS	Oxide Driven System
SACRé	Small Air-Cooled Reactor
SFR	Sodium Fast Reactor
SMR	Small Modular Reactor
SS	Stainless Steel
SSS2	SERPENT (Software, version 2.2.14)

b	Barns
C	Celcius
cm	Centimeter
d	Days
h	Hours
J	Joules
K	Kelvin
Kg	Kilo-gram
KWth	Kilo-Watts
m	Meter
MeV	Mega-electron Volts
MWth	Mega-Watts Thermal

Chemical Element

Al	Aluminum
Al_2O_3	Aluminum Oxide
Ar	Argon
C	Carbon (C-14, C-15)
CH_4	Methane
CO	Carbon Monoxide
CO_2	Carbon Dioxide
Cr	Chromium (Cr-51)
Fe	Iron

FeCrAl	Iron Chromium Aluminum
H	Hydrogen (H-2)
He	Helium (He-3)
K	Potassium (K-41)
Kr	Krypton
LBE	Lead Bismuth Eutectic
$MgAl_2O_4$	Spinel (Magnesium Aluminate)
MgO	Magnesium Oxide
Mn	Manganese
Mo	Molybdenum
N	Nitrogen (N-2, N-14, N-15)
Na	Sodium
Na	Sodium (Na-23)
Ne	Neon
Ni	Nickel
O	Oxygen (O-2)
P	Phosphorus (P32)
Pb	Lead
PbO	Lead-Oxide
S	Sulfur (S-35)
Si	Silicon
SiC	Silicon Carbide
Ti	Titanium

UC	Uranium Carbide
UO_2	Uranium Dioxide
U-Zr	Uranium Zirconium (Metallic Fuel)
V	Vanadium
W	Tungsten
Xe	Xenon
Y	Yttrium
Zn	Zinc (Zn-65)

Math

ɳ	Thermal Fission Factor
N_{fe}	Number of Fuel Elements
P	Pitch
P_{FNL}	Fast Non-Leakage Probability
P_L	Leakage Probability
q_{avg}	Average Linear Heat Production
Q_{th}	Thermal Heat Generation
r_{co}	Outer-clad Radius
r_f	Fuel Radius
V_{core}	Volume of the Core
$V_{f,core}$	Fuel Volume in the Core

TABLE OF CONTENTS

LIST OF FIGURES

xi

xii

LIST OF TABLES

1. INTRODUCTION

1.1 **Small Modular System Selection**

The objective of this thesis is organized towards the design of a small modular reactor (SMR).This selection is made due to some inherent pertinent advantages associated with small and modular system as opposed to large-scaled system.

Small Modular Reactors (SMRs) are nuclear power plants recognized by their small size compared to base load plants and their compact nature [1]. These systems provide power ratings of up to 300MWe [1] and are designed to be built at factories and shipped to the utilities.

SMRs typically require limited on-site preparations and exclude the lengthy construction time innate to large scale nuclear reactors. The integrated nature of these systems allows a lower capital investment, however because of their small size, additional modules can be added incrementally as the energy demands increase [1], which may consequentially lead to an increment of investment. SMRs' flexibility allows this type of systems to be deployed in areas where large systems can't reach, because of limitations in infrastructure, like smaller electrical markets, isolated areas, smaller grids, and sites with limited or no access to water or acreage or unique industrial application [1]. SMRs can be coupled with other energy sources, such as renewables and fossil energy. This ability allows the overall system to weigh resources and operate at higher efficiencies while increasing grid stability and security. Another advantage of these systems is their nonproliferation nature; they are designed to be placed below grade for safety and security enhancements and so forth addressing vulnerabilities to both sabotage and natural phenomena hazards scenarios [1]. By fabricating, defueling and refueling these systems at the factory, the transportation and handling of nuclear materials is limited.

There are presently 131 SMRs currently operating in 25 member states of the International Atomic Energy Agency (IAEA) with a capacity of about 63GWe and 13 SMRs are under construction. They are also 45 innovative concepts for electricity generation and process heat production, desalination, hydrogen generation and other application [2].

1.2 **Fast Spectrum System**

The use of air as a coolant is preferably associated with fast systems because of some characteristics not favorable to thermal systems. The density of air is not high enough to reduce the speed of fast neutrons and turn them into thermal neutrons. Furthermore, air exposed to high temperature is not appropriate in a graphite moderated environment. Air seemingly reacts with hot graphite at temperatures ranging from 500 to 1100°C resulting in chemical reactions that produce O_2, CO and CO_2 in several types of exothermic and endothermic reactions [3]. As a result of that, the graphite will expectedly burn uncontrollably or may severely corrode without the creation of flames.

Adopting a fast reactor for the use of air as a coolant would substantially eliminate the need of any neutron moderating agent such as graphite and also remove the need to slow down neutron. The decomposition nature of air at high temperatures still warrants a need to evaluate and select appropriate material to limit corrosion from the presence of oxygen in the system.

Fast nuclear reactors possess some key advantages in safety, sustainability and waste management. These systems are characterized by a dominant fission caused by neutrons having an energy ranging from ~100keV to the top of the range of the fission spectrum ~15MeV [4]. One of the key advantages of fast reactors is that these systems can be turned to breeder units and thus enhancing their sustainability. These systems can also be made as burner units; they can destroy long-lived nuclear waste by transforming them into nuclides that will decay in centuries rather than hundreds of millennia [5].

1.3 Thesis Objectives

Several designs and analysis efforts are established in order to support the concept of a fast modular reactor, cooled by air. These analyzes implement combinations of reference parameters based on reference designs and reports, and then iteratively adjust the proposed model to meet the performance and design objectives. The overall purpose of this thesis is to evaluate neutronic feasibility of a nuclear system that is cooled by air from the completion of these goals listed below:

- Survey of previous work on the subject of deployable SMRs to justify the size and the mass of the proposed system.

- Evaluation and selection of a suitable fuel that can reasonably achieve a high burnup without producing an excessive amount of High-Level Waste (HLW).

- Evaluation of selected materials that can be exposed to air at high temperature and resist corrosion. This will include the structural, the cladding and reflector materials. This evaluation will include a comparison of the oxidation temperature, melting temperature and a cross-section analysis of their major nuclides.

- The design of a viable modular system that can be appropriately cooled and operable for a desired length of time at a set power level.

- Analysis of the system power unit performance, including an evaluation of the cycle type (open vs. closed), the incorporation and the effect of different types of reflectors on the system, and an overview of alternative system that uses nitrogen as coolant. Nitrogen is selected because it constitutes ~80% of air.

- Analysis of decay analysis of air associated with open cycle system. This will include the assessment of its decay isotopes that can cause health risks to workers.

3

This thesis will be restricted to the reactor physics analysis of an air cooled system. The system design will be limited to a size, fuel mass, cycle length of no more than ten years, and a power of up to 600MWth.

1.4 **Strategy and Modeling Approach**

This thesis will attempt to promote the use of air to cool the reactor. Several materials favorable to reactive and heated air will be evaluated to determine their appropriateness for the system. The question of oxidation will be assessed, and the neutronic feasibility of the system will be determined. The system modeling will be performed with the combination of two codes: SERPENT, a three-dimensional continuous-energy Monte Carlo code [6], and MATLAB, a high-level language for numerical computation, visualization, and application development code [7]. The details of modeling and computational approach are presented in Section 3.2.1 in this report.

1.5 **Thesis Structure**

The thesis presents the characteristics, status, and advantages of compact modular nuclear reactors compared to conventional large scale nuclear reactors.

The thesis follows with a proposal of using air as an alternative coolant for the proposed design. It will include an evaluation of the composition of air and its behavior at high temperatures. To support this proposal, analysis and reviews on materials would be performed to determine their appropriateness in a highly corrosive environment. This study will include the selection of cladding and structural materials.

Finally, this thesis will defend the relevance of the selected configuration of the reactor and will follow with an integration of reflectors. Simulations will be performed with selected

materials to ensure the neutronic feasibility of the reactor and ensure that the system can operate safely in normal operations.

This thesis will mainly focus on material overview and selection, neutronic analysis, and the health evaluation associated with the proposed design. The assessment of this proposed system will be achieved including the combination of computational tools and methods and the coupling and iteration between them. MATLAB will be used to automate the design and assess the obtained results. SERPENT will be used to evaluate the system and weigh on the neutronic feasibility of the proposed design. This will include the full core modeling, the fuel cycle analysis, and the system performance evaluation.

2. GAS FAST REACTOR

2.1 Introduction to Gas Fast Reactors

Gas Fast Reactors (GFR) represents an alternative to the very common and prevalent Sodium Fast Reactors (SFR) or the Lead-cooled Fast Reactors (LFR) [8]. Designs for GFR began development in the United States and Europe as an alternative to liquid-cooled fast reactors during the 1960s through 1980s [5].

GFR leads to a harder neutron spectrum than heavy liquid metal cooling or sodium, therefore allowing a higher breeding ratio and a shorter doubling time relative to the liquid metal cooled reactors, when high power densities are maintained [8]. The initial concept, from General Atomics in 1962 included preliminary designs of a 300MWe demonstration plant and a 1000MWe commercial power plant. These models included a range of core design configuration with metal clad pins using oxide or carbide fuel [8].

Analysis and comparison between steam, carbon dioxide (CO_2) and helium lead to the selection of helium for current gas fast reactors. Steam was rejected due to cladding compatibility problems, positive coolant reactivity effect and reduced breeding performance. CO_2 provides a higher pressure drop, increased acoustic loadings and economic penalties associated with a required increment of the primary coolant pumping power [8]. However, there have not been many researches of potential design that include air or nitrogen as a coolant.

Some of the potential elements susceptible to affect the performance of gas-cooled reactors include the heat transfer across flow channels, loss of coolant or depressurization accidents. These elements can result in core damage in the event that passive/inherent safety systems are relied upon post transient decay heat removal [8].

2.2 Selection of Air as Primary Coolant

The abundance of air in nature facilitates the replacement of helium or sodium, and so forth would eliminate the need for any storage and resupply tanks. Also, in the event of a depressurization-loss-of-coolant-accident (DLOCA), assuming that the system can indeed be designed to use air as its coolant, there would be no complications resulting from an inability to maintain helium circulation, even at atmospheric pressure [4]. There would also be no complications from an air ingress, since the GFR, unlike the High-Temperature Reactor, would not contain graphite [4].

Air has many advantages similar to helium, compared to liquid coolants. Air, like helium, does not have a violent chemical reaction in the event of a leak (unlike sodium, which reacts with air and water) [9]. Air is optically transparent, enabling easier inspection and repairs [9]. Air also allows simplifications of the cycle and the removal of complexities from having two-phase flow. While air's neutron transparency is not as desirable as helium's, it is still far better than sodium (as presented in Table 1 with a better void coefficient), its activation has a fission-spectrum average cross section of 225.8 μb and results in the emission of two gamma rays: 2.754 MeV and 1.393 MeV, with a half-life of 14.959 hours [10]. The trace argon (0.933% by volume [11]) in the air activates with a microscopic cross section of 1.013 mb and usually emits a 1.294 MeV gamma ray with a 109.34 minute half-life [10].

The use of air allows the possibility of operating a reactor in a direct cycle (Brayton cycle) as opposed to sodium cooled nuclear reactor (SFR), which requires two to three loops [12]. This ability is due to the activation of air not carrying severe concerns to the cycle as opposed to sodium. A second benefit necessary to be accounted for is the low void coefficient of gas coolant owing to the low rate of neutron capture [9]. Because of the low radiative neutron capture in gases, nuclear systems with a small void coefficient than SFR can be designed.

Table 1 also shows some of the pertinent advantages of helium over the air; helium has a favorable ability to transfer heat across the channel, and its light weight allows it to flow with minimal pumping power. Air does, however, have a competitive heat transfer per unit volume compared to that of helium. A given volume of air will have a similar heat capacity to a same amount of helium, but different respective masses. Nuclear systems are characterized by a fixed amount of coolant space while the mass of the coolant within the reactor varies with pressure.

Table 1. Properties of Coolants at Atmospheric Pressure [10], [13].

`	Helium Properties (273K)	Air Properties (273K)	Sodium Properties (273K)
Thermal conductivity [W/mK]	0.149	0.0257	66.1
Density [g/cm^3]	0.00018	0.00128	0.842
Specific heat capacity [J/KgK]	5188	1005	1272
Dynamic viscosity [Kg/ms]	2.00E-05	1.1805E-05	3.46E-05
Prandtl number	0.696	0.462	0.00067
Reynolds number relative to Helium (for a given channel diameter and velocity)	1	12	2704
Radiative capture (n,γ) cross-section of interest*,δ_γ (fission spectrum average) [b]	N/A	1.01E-03	2.26E-04
Half-life **	7.6E-23 [s]	1.822 [hr]	14.959 [hr]
% yield of γ decay mode **	N/A	99.16%	100%
Heat capacity per unit volume [J/cm^{3}K]	0.000934	0.00123	1.07
Decay γ energy** [MeV]	N/A	1.294	2.75, 1.39

Another advantage of air over helium is its dominance in turbo-machinery manufacturing. The majority of design machines are manufactured with air/steam as opposed to helium. There are only three historical examples of helium turbines, and only two of these were coupled to nuclear reactors [14]. All other historical helium-cooled reactors have transferred their heat to a secondary working fluid. The difficulties with helium turbo-machinery arise mostly because of two factors. The first one being helium's low molecular weight; it allows air to move towards undesirable pathways including diffusion through heavy materials, leakage from the system, and leakage within the system causing some components to receive less than optimal coolant flow [14]. Furthermore, a multi-stage compressor-turbine assembly is typically necessary to achieve a high compression ratio with helium compared to air, leading to unpredictable harmonic disturbances along the axis of the assembly [14]. Air-driven turbo-machinery, however, can easily be derived from experience in the natural gas industry [15].

Gas cooled systems do however carry some drawbacks. These include a limitation of the performance and efficiency of the nuclear system during normal operation [5]. The low thermal, inertia prone to gas cooled nuclear reactor, warrants the need to evaluate the safe and efficient dissipation of decay in the event of an accident, to avoid a similar control problem as to Fukushima meltdown.

Helium's high thermal conductivity and specific heat are two characteristics that make helium the most commonly used gas coolant for fast nuclear systems but the higher density of air goes a long way toward making its cooling capability competitive with that of helium. The purpose of this study will not be to compare air coolant to helium, nor will it be to shun its usability, but merely to introduce an alternative to it, which is air and promotes some of its economical and neutronics competitiveness.

3. COMPUTATIONAL TOOLS AND SYSTEM ANALYSIS

3.1 Computational Tools

The evaluation of the proposed system will be performed with the combination and iteration between SERPENT and MATLAB.

3.1.1 SERPENT

SERPENT is a three-dimensional continuous-energy Monte Carlo reactor physics code [6] that is being developed at VTT Technical Research Centre of Finland since 2004. The version of Serpent used for the simulation of the results of this thesis is Serpent 2.2.14 (SSS2). Its applications include the generation of homogenized multi-group constants for deterministic reactor simulator calculators, fuel cycle analysis involving detailed assembly level burnup calculations, reactor physics analysis, and neutron tracking [6].

SERPENT uses a universe-based combinatorial; solid geometry model, similar to MCNP (Monte Carlo N-Particle code, used for neutron, photon, electron, or coupled neutron/photon/electron transport) and KENO-VI (an extension of the KENO Monte Carlo criticality code, mainly used to determine k_{eff}, the lifetime, generation time, energy dependent leakages, energy and region-dependent absorptions, fissions and fission densities), which allow the description of practically any two or three dimensional fuel or reactor configuration [6]. The burnup capability in SERPENT is entirely based on the built-in calculation routines, without any external coupling [6]. The number of depletion zones is not restricted, although memory usage may become a limiting factor when the number of burnable materials is large [6].

SERPENT will be used to model the core and analyze the neutronic of the system. These include criticality analysis, spectrum evaluation, flux mapping and analysis and power distribution analysis for the full core and selected assemblies.

3.1.2 MATLAB

MATLAB (MTL) provides a range of numerical computation methods for analyzing data, developing algorithms, and creating models. MATLAB language includes mathematical functions that support common engineering and science operations. Core math functions use processor-optimized libraries to provide fast execution of vector and matrix calculations [7]. MATLAB scripts will be used to control the simulation with SSS2. The MTL control system will iterate on k_{eff}, reflector material, and fuel enrichment to come up with the appropriate configuration. MTL will also be used to analyze SSS2 simulated results and generate plots.

3.2 Analysis Methodology

3.2.1 System Design Approach

Having selected some potential materials (clad, reflector and structural) pertinent to the design of the proposed system, the analysis will be simulated iteratively with SERPENT and MATLAB to determine the appropriate configuration for the system. The depiction of this iteration is presented in Figure 1. Literature surveys and analysis will be evaluated extensively to determine the appropriateness of the pre-defined configuration of the pre-conceptual model. The system volume for all its constituents will be optimized primarily with a set fuel rod diameter and, rod and assembly pitch. The rod cladding material and the system's reflector will be secondarily evaluated before moving to the system's safety and the cycle evaluation.

The analysis details are presented in Figure 1. Each section will contribute to the optimization of the pre-defined system and the selection of the appropriate configuration to satisfy the object of this thesis.

The system thermal power will be set, and the transportability requirement of the proposed system will assist in the definition of the size of the reactor, which in turn will define the core loading. The core loading will be determined such that the system can run for an extended length of time before being reloaded.

The fuel loading will be evaluated with a single enrichment and the reflector material will be assessed for a system that provides an appropriate power distribution. The system will be modeled with sufficient and adequate fuel and coolant volume fraction. .

3.2.2 Core Neutronics Modeling Approach

A number of steps will be taken to evaluate the core and attain to final configuration of the system, favorable to the neutronic aspect of the design. These actions will encompass series of simulations and analysis with SERPENT (SSS2), programmed and automated by MATLAB (MTL). These measures are presented as follows:

- Literature survey on existing and conceptual gas reactor rod dimensions. Air is anticipated to be poor coolant compared Helium, designing a system with smaller rod diameter would be beneficial and advantageous. Assume fuel, coolant and clad temperature and pressure for the material.

- Study and literature research on a list of potential materials cladding, reflector material and structural and system casing material

- Design and simulation of an infinite lattice to evaluate the spectrum and determine the appropriate cladding material

12

Figure 1: System Design Approach Diagram.
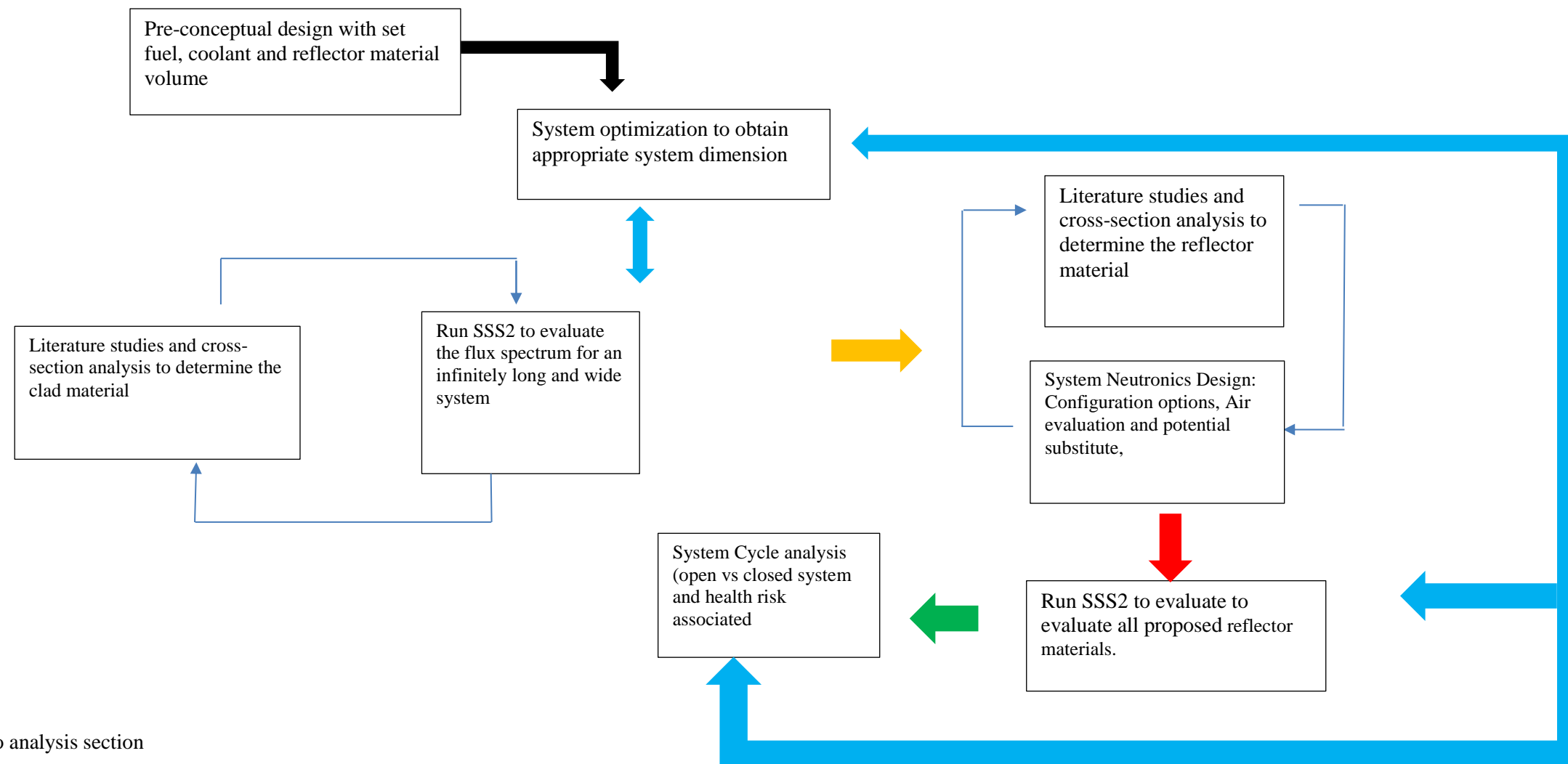
BLACK: Move to analysis section

BLUE: Optimization steps

YELLOW, **RED**, **GREEN**: Optimized Element 1 Optimized Element 2 and Optimized Element 3.

- Literature survey on existing core dimensions and reactor height specification. The set height of the core must be conducive and favorable to ground transportation. It is desired to fit the core and its constituents in a 20ft container.

The following steps will be performed for the different types of reflector material; they will be automated with MTL. MTL will be used to visualize and analyze the results obtained.

- Design the core lattice and control rod positions in the system. Run SSS2 to ensure that with rod fully inserted into the system, the reactor is subcritical. This analysis will contribute to insuring that if an unsolicited event was to happen, the core can be shut down safely, and the system will be subcritical.

- Run SSS2 to determine the criticality, k_{eff} of the system. The criticality calculation will be run several times, with increasing fuel enrichment, to ensure that there is enough excess reactivity to ensure that the system will be able to run for a desired amount of time before being reloaded.

- Run SSS2 with Burn Card active to simulate the system's irradiation and to determine the cycle length of the proposed system.

- Compare the results obtained with MTL to determine the appropriate reflector material for the proposed system.

- The system's cycle will be evaluated with SSS2, and literature research and studies. Air will be irradiated with SSS2 to assess the isotopes produced from its constituents' activation. Several studies will be performed to determine their decay time and determine if these elements will impede the worker's health in an open cycle. The system's cycle will be evaluated theoretically by the efficiency and safety concerns.

3.2.3 System Analysis

The system's geometry, the materials configuration modeled with SSS2 and some formulas presented in this section will be linked and compiled with MTL to evaluate the system and satisfy the requirements laid out in this thesis.

3.2.3.1 System Geometry Evaluation

The pre-selected dimensions of the fuel element, including the radial and axial dimension along with the self-imposed height of the active core H, and the radius of the fuel material r_f, will enable the computation of a single fuel rod volume as follows:

$$V_f = \pi r_f^2 H \tag{1}$$

This value, along with the number of fuel elements, N_{fe} modeled in SSS2 will enable to computation of the volume of the core as presented below:

$$V_{f,core} = V_f N_{fe} \tag{2}$$

The volume of the fuel element, with r_{co} defined as the radius of the outer clad is calculated with the following equation:

$$V_{fe} = \pi r_{co}^2 H \tag{3}$$

The pitch-to-diameter ratio used to model SACRé will not be optimized upon. This value will be determined about the range of value of typical fast reactors. The upper value of the P/D ratio will be no more than 1.5 [16], while the theoretical lower limit will be not less than 1.0.

The total cross-sectional area of the active core is defined as:

$$A_{core} = \frac{p^2 N_{fe} \sqrt{3}}{2} \tag{4}$$

The total volume of the active core is calculated by the following equation:

$$V_{core} = A_{core}H \tag{5}$$

This calculation is performed while taking into account the physical presence of the control rod subassemblies in the system.

The equations presented above will help determine the volume occupied by each element and materials in the core. These include the fuel material, structural material, control rods (primary and secondary), reflectors (axial and radial) and shield (axial and radial). This analysis will not include the model of the wire wrap around the fuel element.

3.2.3.2 Heat Production Analysis

The average linear heat production rate is defined as the total thermal power production in the core divided by the total length of all fuel rods in the core [4]. The formulation is presented as:

$$q'_{avg} = \frac{Q}{N_{fe}H} \tag{6}$$

The maximum linear heat production in the core is found by multiplying the average rate by the power peaking factor from the neutron flux profile [4]. This analysis is summarized in the following equation:

$$q'_{max} = q'_{avg}F_q \tag{7}$$

The heat rate, heat flux and the power peaking factor will be obtained from SSS2.

4. POWER UNIT PERFORMANCE CHARACTERISTICS

4.1 Air Behavior in High-Temperature Reactive Environment

Selecting air as a potential fast reactor coolant for the feasibility of SACRé warrants the need to understand its behavior in a reactive and heated environment. The important components to evaluate in this event are the oxidation and the activation analysis of its isotopic constituents. Air is relatively highly corrosive because of the high concentration of oxygen. The composition of air is presented in Table 2.

Table 2. Air Composition by Percent Volume [17].

Gas	Formula	Presence
Nitrogen	N	78.084%
Oxygen	O_2	20.9476%
Argon	Ar	0.934%
Carbon Dioxide	CO_2	0.0314%
Neon	N	0.001818%
Methane	CH_4	0.0002%
Helium	He	0.000524%
Krypton	Kr	0.000114%
Hydrogen	H_2	0.00005%
Xenon	Xe	0.0000087%

Oxidation is defined as the reaction of metals and oxygen [18]. This event is best known as dry corrosion, which occurs from the reaction of air with metal without the presence of a liquid [19]. Dry corrosion is typically not as detrimental as wet corrosion, observed in reactor cooled with liquid such as water [19]. Dry corrosion is very sensitive to temperature [19]. In a highly oxidizing environment, like in SACRé system, oxide layer will be formed continuously

around the metal separating the fuel from the coolant (fuel cladding). There are cases where dry corrosion is encouraged. The oxide layer being formed on the surface of the metal will lead to a reduction in the rate of corrosion [20]. In some other cases, dry corrosion may possibly lead to combustion, like in graphite environments [21]. This layer can consist of oxides of iron, chromium and other element depending of the composition of the material [17].

Up to a certain temperature, known as the scaling temperature or maximum service temperature, the oxide layer is continuous and dense, and protects the underlying material from high-temperature corrosion attack [18]. Above the scaling temperature the layer tends to crack and will, therefore, lose its protective capacity [18].The difference in oxidation rates depends on the conductivity of the oxides because the ions have to move through the oxide layer [20]. Oxidation occurs much more rapidly as the temperature increases because the mobility of ions within the oxide layer increases [19]. The phenomenon is presented in Figure 2 below.
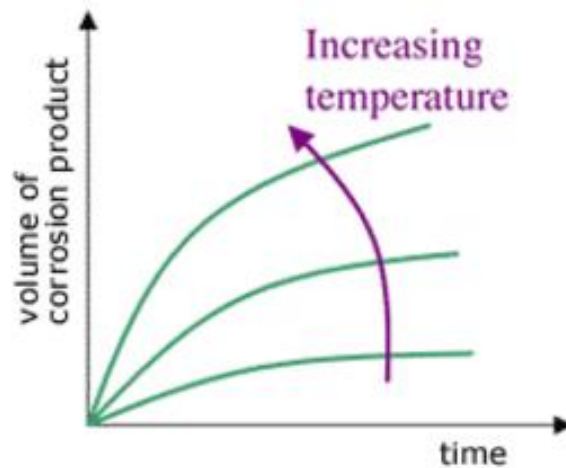
Figure 2. Rate of Corrosion over Time with Increasing Temperature [19].

18

Selecting the appropriate material for the design of SACRé for the fuel clad, reflector and structural material will be necessary to enhance a controllable oxidizing environment.

Another important component to account for, in an environment similar to that of SACRé, is the coolant activation with neutrons and the decay of some of its constituents. This analysis is significant especially if the proposed system was designed to feature an open cycle where activated air is likely discharged in the environment. Some of the radionuclides from the activation of air are likely to pose a threat to human, especially the maintenance workers. The Health Physics and Radiological Health Handbook list about 300 target/product pairs in its neutron activation database [22]. A limited amount of these activation products will be evaluated in this study because of their significant potential for dose to workers. These radionuclides includes: ^{32}P, ^{35}S, ^{41}Ar, ^{51}Cr and ^{65}Zn. The activation of air will be evaluated with SERPENT in order to attempt to evaluate the rate of production.

4.2 System Power Cycle Evaluation

One of the advantages of a gas cooling system (air in this thesis) is the possibility that this coolant gas can be used directly as a working fluid in the thermodynamic cycle. This option is available through the Brayton cycle. The Brayton cycle can eliminate the need for multiple coolant loops. This cycle allows the operation at higher temperatures, hence higher cycle efficiencies [23]. In this thesis, two forms of direct Brayton cycle will be considered: the closed Brayton cycle and the open Brayton cycle.

4.2.1 Closed Cycle Design

The proposed closed Brayton cycle is a cycle through which the volume of air in the system is preserved. This cycle includes a turbine, a compressor, a cellular recuperator and some pumps. In this cycle, heated air from the reactor is fed directly to the turbine. This hot air will go

through a cellular recuperator, where it will lose some fraction of its temperature, then through a heat exchanger also known as a cooler. From the cooler, cooled air is fed through the compressor, then through the cellular recuperator before serving as a coolant for the system. The energy is lost in the recuperator from the partial interaction between cooled air from the compressor and hot air from the turbine and in the air cooler, from the partial interaction with chilled air from the environment. This system integration is presented in Figure 3. A pertinent attribute to this system is that it is more controllable; the activated air is contained in the system.
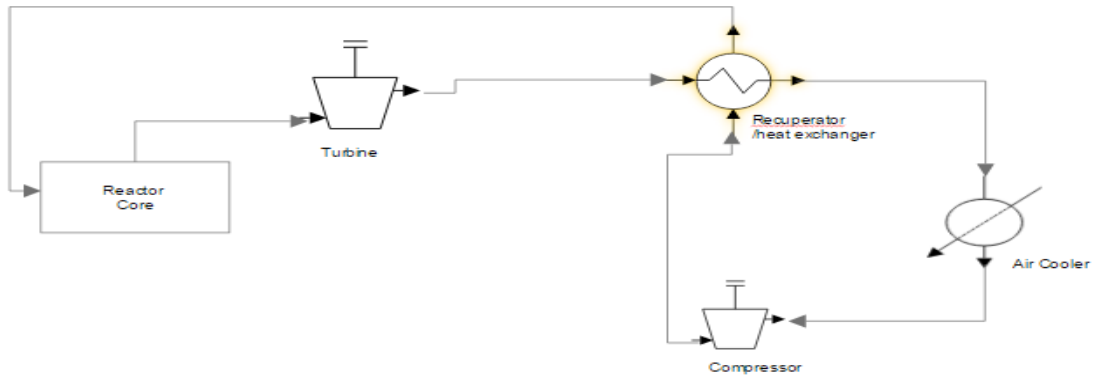
Figure 3. Closed Brayton Cycle of SACRé system.

The cellular recuperator, also known as cross plate heat exchanger, is selected for the design of this system because its 85 -99% efficient [24]. SACRé system is envisioned to be compact and the entirety of the system is expected to be incorporated into a system.

4.2.2 Open Power Cycle Design

In the proposed open cycle of SACRé system, air is continuously replenished into the system. Atmospheric air is taken through a filter then through the compressor. Then moderately

heated air is taken through a cold end of the cross plate heat exchanger (cellular recuperator) to increase its temperature and pressure into a desired value before being fed into the reactor. Heated air (steam) moves from the reactor directly to the turbine then through the hot end of the recuperator before being discharged in the atmosphere. That hot air will serve as a heating agent to increase the temperature of air from inlet from atmosphere before being fed in the recuperator/heat exchanger then to the reactor. The system integration is presented in Figure 6 below. A pertinent attribute to this system is that conventional heat exchanger is eliminated from the system, thus lower maintenance cost, capital investment and power consumption.
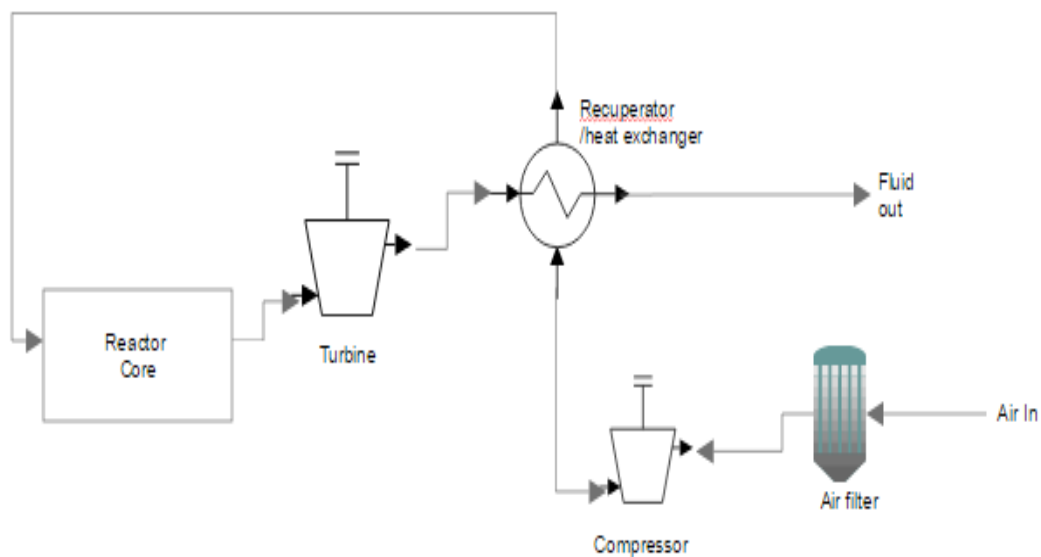
Figure 4. Open Brayton Cycle of SACRé System.

4.3 **Production and Atmospheric Release of Activation Products from Air**

Designing a system with an open cycle warrants the dire need to evaluate the nuclides produced from the activation and irradiation of air. The Health Physics and Radiological Health Handbook lists about 300 target/product pairs in its neutron activation database [25]. A limited amount of these activation products will be evaluated in this study because of their significant potential for dose to workers. These radionuclides includes: P-32, S-35, Ar-41, Cr-51 and Zn-65. Their half-lives range from 1.8 hours to (Ar-41) to 244 days (Zn-65). These isotopes were selected because they have potential for the most significant human exposure [25]. Table 4 lists characteristics of these target isotopes.

Table 3. Characteristics of Target Nuclides [25].

Radionuclide	Primary Product Isotopes	Half-life	Beta Energy (MeV) max	Gamma Energy (MeV)
P-32	P-31	14.3 d	1.7	None
S-35	Cl-35	87.3 d	0.17 (100%)	None
Ar-41	Ar-40	1.43 h	1.2 (99%)	1.29 (99%)
Cr-51	Cr-50	27.7 d	Electron Capture	0.32 (9%) 1.17 (100%)
Zn-65	Zn-64	244 d	Electron Capture	1.12 (49%)

SACRé system was simulated with SSS2 to evaluate and analyze the flow of activated air around the system. This analysis was done with the closed cycle system to determine which nuclides will be dominant among the selected nuclide to be evaluated. This analysis was done by irradiating air in the core and evaluating the production and decay time of those key isotopes. The production of these isotopes in the system is presented in Figure 5. The evaluation of the

activation of air in the system exposes a significant dominance in the production of Ar-41 from the system. Its dominance in the system makes it the primary activation product of interest in terms of airborne release and potential offsite dose. The apparent non-existence of the other target isotopes investigated lead to a dire need to individually observe each of these elements. Plots of individual target isotopes are presented from Figure 6 to Figure 10.

A survey of the production and magnitude of the selected target isotopes from the irradiation of air lead to the focus of the study on Ar-41. A comparison of the atom density per cycle length of these isotopes presents a difference of an order of magnitude. It can be derived from this observation that Ar-41 is the main isotope to watch for, for the workers working around the plant.
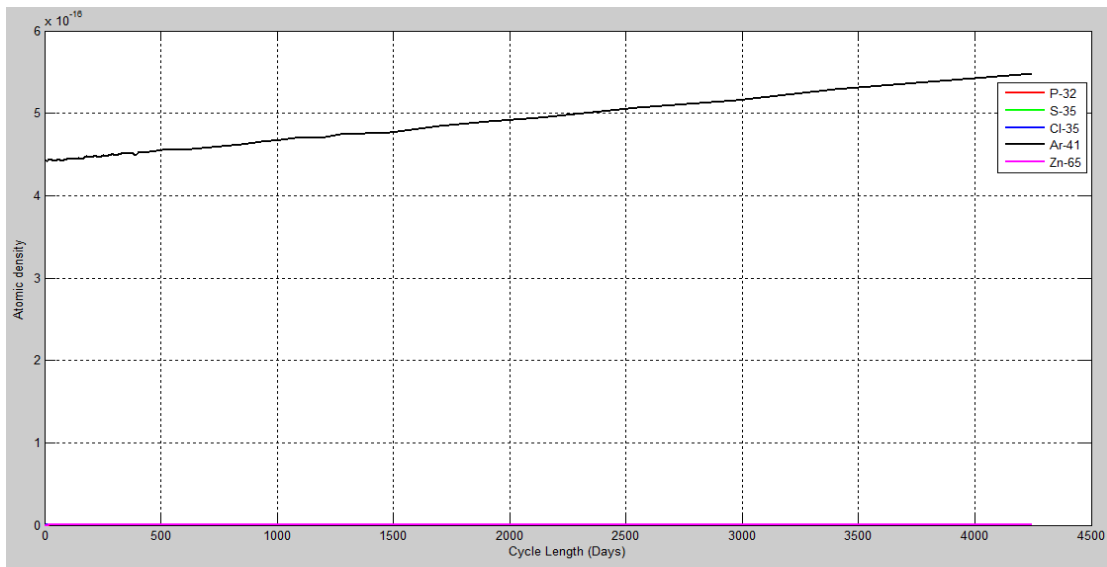
Figure 5. Production of All Key Isotopes per Cycle Length.
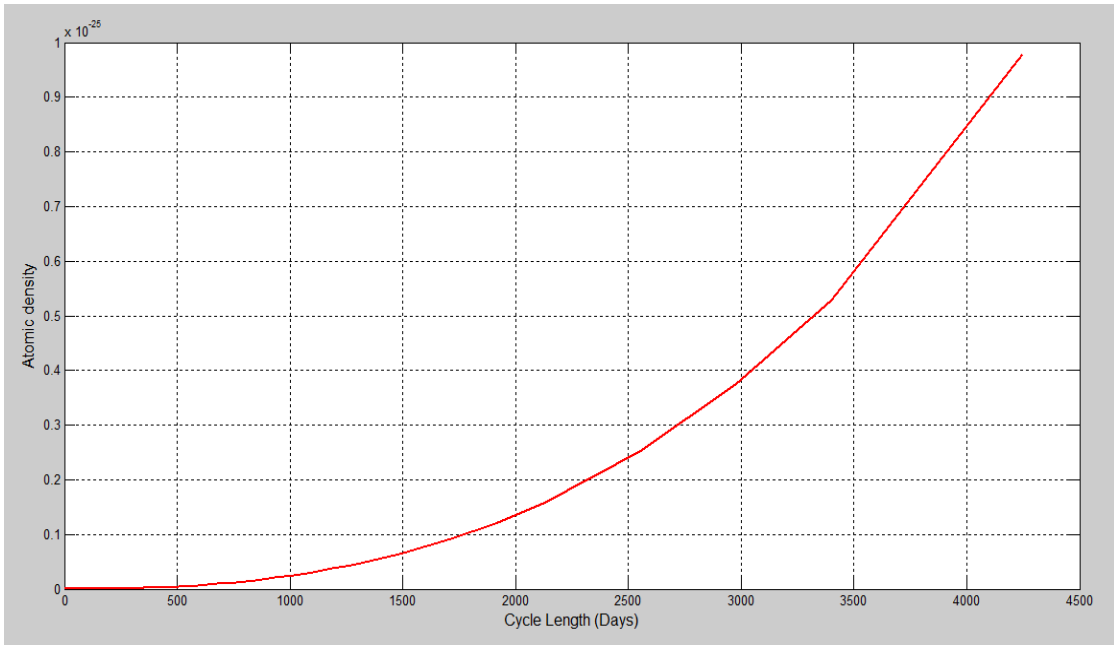
Figure 6. Production of P-32 per Irradiation Length.
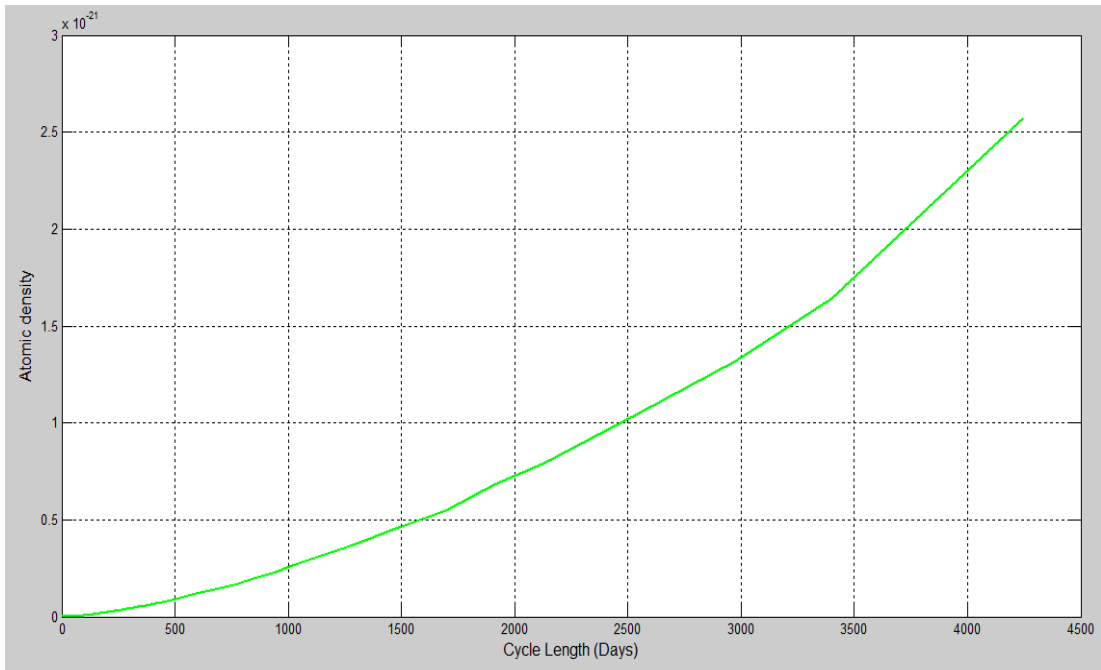
Figure 7. Production of S-35 per Irradiation Length.
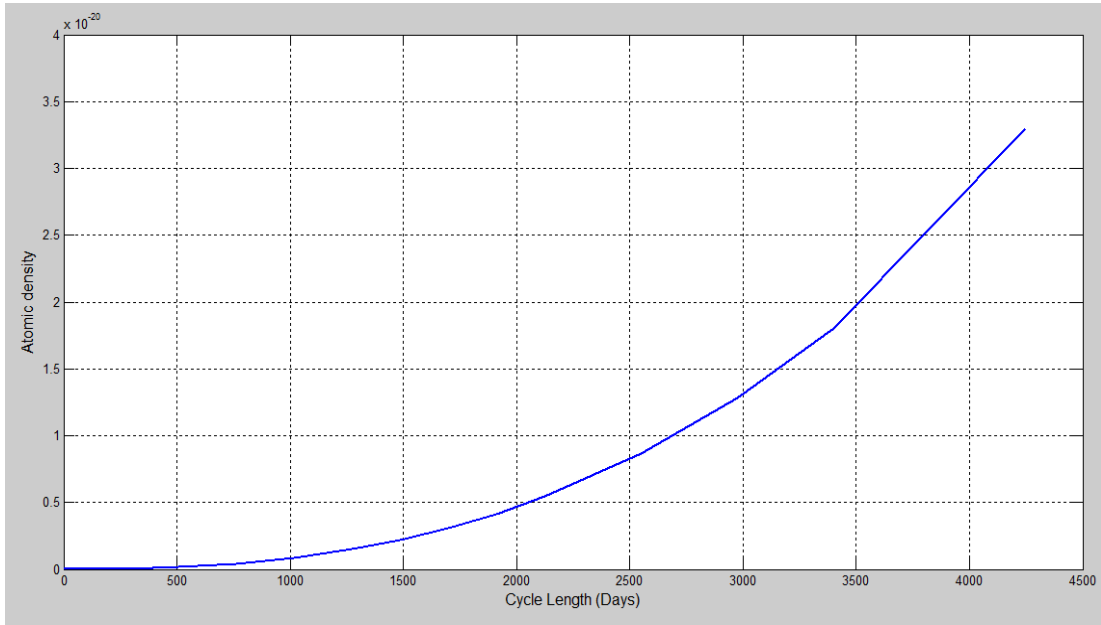
Figure 8. Production of Cl-35 per Irradiation Length.
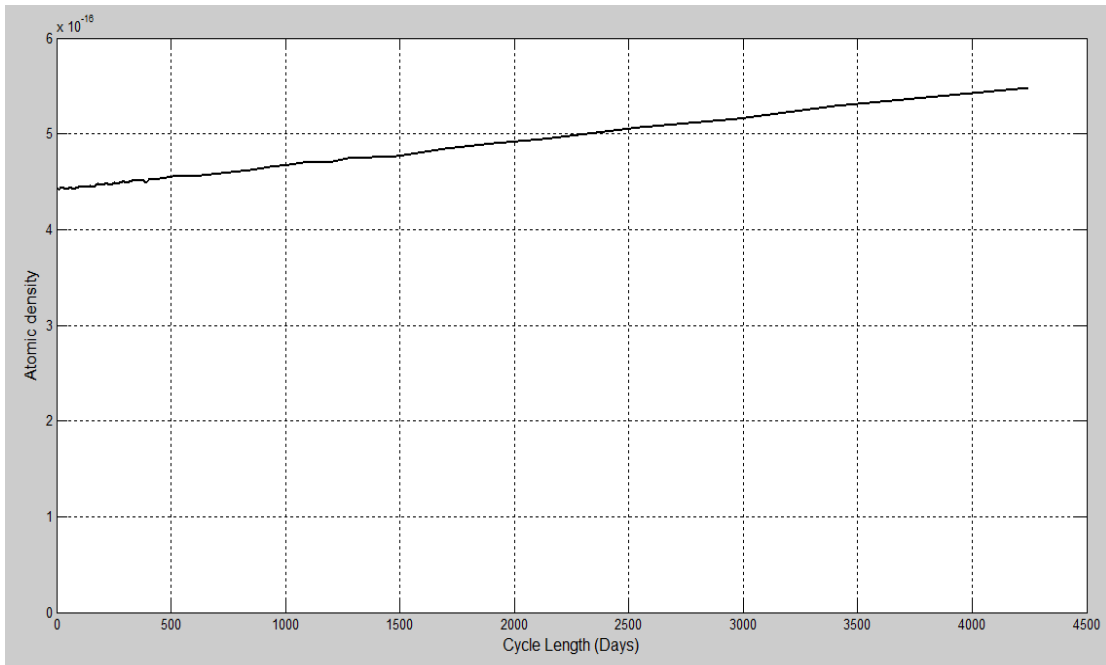
Figure 9. Production of Ar-41 per Irradiation Length.
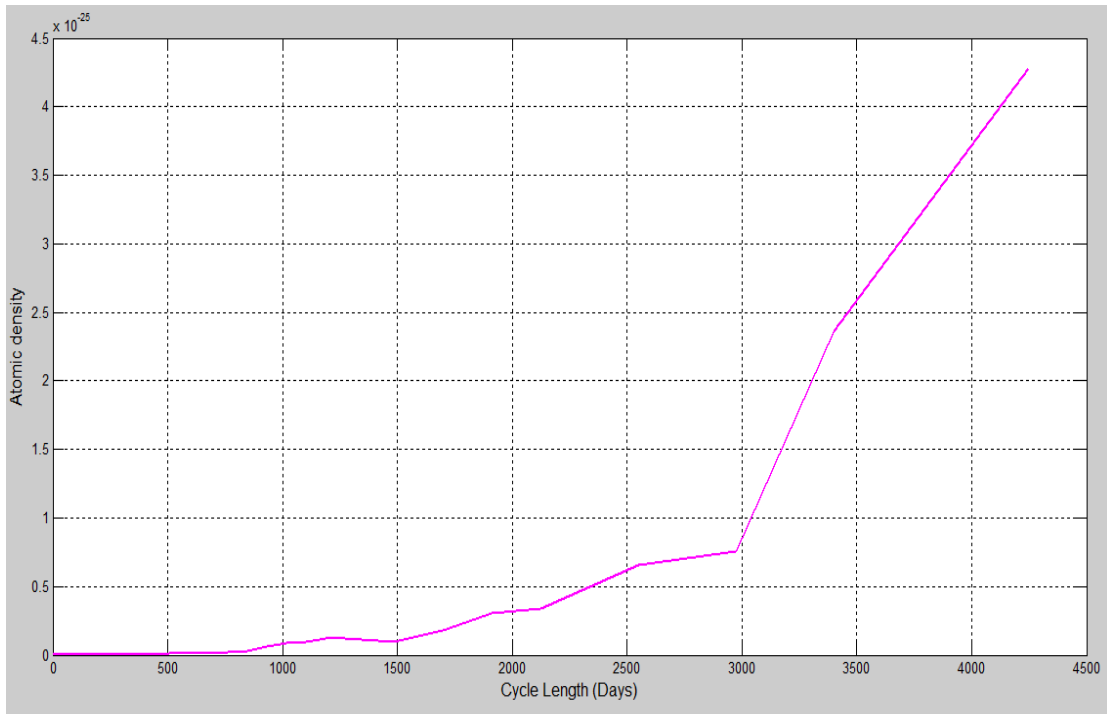
Figure 10. Production of Zn-65 per Irradiation Length.

Ar-41 is primarily produced from the interaction of neutrons with Ar-40, which is present in air and disintegrates by beta minus decay to excited level and the ground state level of potassium-41 (K-41). Figure 11 presents the decay the decay scheme of Ar-41.

The likely most common exposure of offsite workers with this noble gas will be through inhalation. LENNTECH reports that the most common effect of such exposure can be dizziness, dullness, headache, nausea and death, which may results from error in judgments, confusion or loss of consciousness [26]. The low half-life of Ar-41 allow several options and possibilities to delay its release with different system configuration in such a way that by the time that activated air is release, there's a relatively limited to no amount of Ar-41 in the fluid.

26

A potential configuration for an open system may include a tank where irradiated air (high concentration of Ar-41) is stored then pushed through some small air channels tubes then upwards in the environment or underground; the sole purpose of any configuration is to delay the flow rate until release without affecting the mass flow rate necessary to cool the reactor.
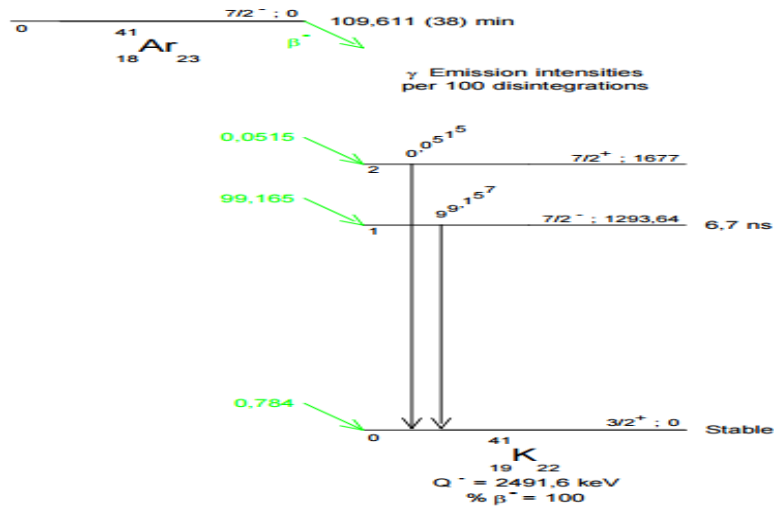
Figure 11. Decay Scheme of Ar-41 [27].

4.4 **System Material Survey**

The chemical reactivity of the oxygen component of air, especially at high temperatures, necessitates that the fuel cladding reflector and other structures in the core be oxidation resistant in addition to neutron-transparence. This obstacle can likely be overcome, since nuclear industries already routinely subject metals to highly corrosive environments in LWRs [28], and the development of super-alloys is an ongoing interest.

Increasing the amount of chromium (Cr), silicon (Si) and Aluminum (Al) in a material increase the resistance to oxidation [17]. The addition of rare earth metals and reactive elements such as titanium (Ti), zirconium (Zr) and yttrium (Y) has a positive effect on oxidation resistance [17]. Despite being appropriate recommendations to limit the rate of oxidation in the system, their effect when exposed to neutron should be duly assessed.

4.4.1 Clad Materials

Resistance to corrosion is an important quality to analyze when choosing the fuel element cladding material. In fast reactor, thermal neutrons are of less importance as opposed to fast neutrons leading to the popularity of stainless steel material. The type of stainless steel should however be properly evaluated; some stainless steel corrodes quickly and are not suitable for prolonged exposure to air at high temperature [29]. Reviews of previously performed material's oxidation yielded the selection of potential candidates for fuel clad materials. These materials and their thermo-physical properties are presented in Table 4. All these materials exhibits a high resistance to oxidation; their oxidation temperature range from 800°C (FeCrAl) to 1700°C (SiC). These materials have a high melting temperature, making their selection appropriate for the design of SACRé system. The composition of these alloys is presented in Table 17 of the Appendix.

Table 4. Potential Cladding Material for SACRé System.

	FeCrAl	SiC	304SS	310SS	316SS	APMT	Inconel 718
Oxidation temperature	~800 C [30]	~1000-1700 C [31]	~816 C [32]	~1100 C [33]	~816 C [32]	~1300 C [34]	~1380 C [35]
Melting temperature	~1500 C	2730 C	~1399 - 1454 C	~1354 - 1402 C	~1399 - 1454 C	~1500 C	~1260 - 1336 C [36]
Density [g/cm^3]	7.1	3.2	7.9	8.03	7.9	7.3	8.19

4.4.2 **Reflector Materials**

There are not enough report on pertinent reflector material's oxidation analysis when exposed to an environment similar to the one suggested in this thesis. There's however a possibility to clad the reflector material to ensure that the oxide reacts with that barrier rather than the reflector material. The cladding material must however be transpicuous to neutron, both high and low energy neutrons to ensure a high efficiency of the reflector material. The selected reflector wrapping material will be the same as that of the fuel clad and its sole purpose will be to hold oxidation reaction away from reflector material. This approach was selected due to the lack of research of oxidation evaluation of some potential reflecting material.

Table 5. Thermo-Physical Properties of Potential Reflector Materials [37].

Properties	Pb	$MgAl_2O_4$ [38]	LBE	PbO	MgO	Al_2O_3
Density (g/cm^3)	11.34	3.58	10.15	9.3	3.401	3.95
Boiling Temperature (°C)	1745	2135	1670	1477	3600	2977
Melting Temperature (°C)	327.4	2135	125	888	2582	2072
Heat Conduction (W/mK)	15.4	5.4-14.7	14.2	1.3-2.2	45-60	18

Several studies of reflector materials were evaluated to determine the appropriate one for this system. This evaluation yielded to the selection of Magnesium-Oxide (MgO), Lead-Oxide

(PbO), Lead-Bismuth Eutectic (LBE), Magnesium-Aluminum Oxide (MgAl$_2$O$_4$), Lead (Pb), and Aluminum Oxide (Al$_2$O$_3$). The Thermo-physical properties of these reflector materials are presented Table 5.

Table 5 shows that lead based alloy such as LBE have a relatively low melting temperature compared to pure lead. PbO has the highest melting temperature among all the lead based reflectors considered in this study. The melting temperature of these material can be overlooked as these materials will be in a casing material, prohibiting it from spreading everywhere in the reactor. The chemical compositions of these materials were obtained from the material datasheet by Pacific Northwest National Laboratory [39]. The oxidation temperatures of these materials were not defined in this thesis; there is a lack of research in that area. Because these reflector materials will be cladded with a separate oxidation resistant material, some assumptions can be made that the reflector materials will be safe from any oxidation reaction since the coolant will not directly interact with these materials.

4.4.3 Structural Material Review and Selection

Appropriate structural materials need to endure much higher temperature, high neutron doses and extremely corrosive environment, as advertised in SACRé system. Several researches on gas fast reactors promoted the focus of studies to ferritic/martensitic steels, austenitic stainless steels, refractory alloys and ceramics [40]. Table 6 presents the types of material for each type of Gen-IV reactors [29].

The selection of the appropriate structural material for this system will be based on some key characteristics like an excellent dimensional stability against thermal and irradiation creep and/void swelling, favorable mechanical properties like strength, ductility, creep rupture, fatigue, creep-fatigue interactions. Acceptable resistance to radiation damage (irradiation hardening and embrittlement) under high neutron doses and high degree of chemical compatibility with high

temperature air/steam to limit the degree of stress corrosion cracking and irradiation assisted stress corrosion cracking [29].

Table 6. Summary of Various Candidate Structural Materials for Gen-IV Reactors [41].

Reactor System	F-M Steel	Austenitic S.S	ODS Steel	Ni-base alloys	Graphite	Refractory alloys	Ceramics
GFR	P	P	P	P	-	P	P
Pb-LFR	P	P	S	-	-	S	S
MSR	-	-	-	P	P	S	S
SFR	P	P	P	-	-	-	-
SCWR	P	P	S	S	-	-	-
VHTR	S	-	-	P	P	S	P

P = Primary, S = Secondary

A study sponsored by the Department Of Energy (DOE) on Gen-IV structural materials promoted the selection ferritic/martensitic steels These alloys have good high temperature properties, radiation resistance in terms of swelling and radiation embrittlement. A prime example of the selection of this material for SACRé casing is HT-9 steel. Table 7 below present the composition of these materials

Table 7. Chemical composition of HT-9 Steel [42].

Material	Weight Fraction
Ni	0.5%
Cr	12%
Mn	0.2%
Mo	1%
Si	0.25%
W	0.5%
V	0.5%
C	0.2%
Fe	84.85%

4.5 **Potential Substitute of Air**

The presence of oxygen in the air contributes greatly to the challenges of using this fluid as a potential coolant, however because of the dominance of nitrogen (N-14) in it, this isotope can be considered as a potential substitute to cool the reactor.

N-14 has a higher specific heat capacity per unit volume than helium [43]. One of the activation products from the exposure of nitrogen to neutron is nitrogen (N-15). Because of a large presence of scattered photons, an isotope expected to be observed is carbon (C-14), which is an easy material to store, isolate and handle [43]. A simulation of the system with configuration presented in Section 5.2.1 was performed to determine the most dominant isotope among the three mentioned above. The result obtained in presented in Figure 12. The results obtained presents a dominance of N-14 compared to N-15, C-15 and C-14. This observation lead to the belief that it would be more appropriate to make this system closed as opposed to open. The coolant would be contained in the system. This may in fact lead to the presence of storage tank around the system. This pertinent attribute may lead to some drawbacks associated with the design of this system.
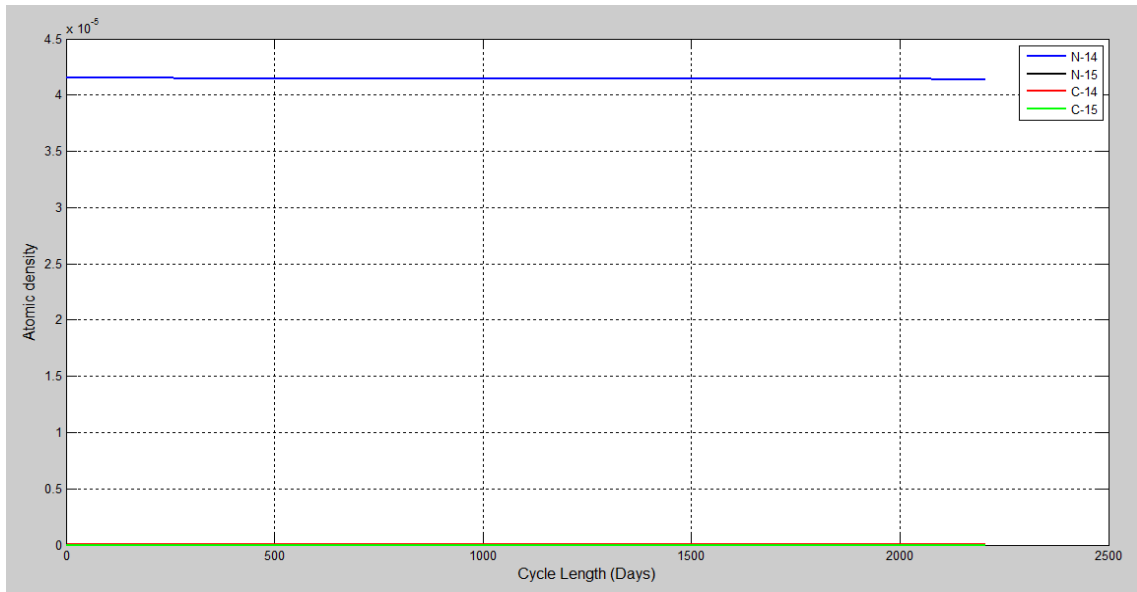
Figure 12. Isotopic Analysis of the Nitrogen Cooled System.

There are various ways to separate air to obtain an oxygen free fluid. An example of this technique and process is known as cryogenic air separation units (ASU) [44]. This unit can be connected to the system, where atmospheric air is processed and nitrogen extracted and directly injected into the secondary loop to cool the reactor. The illustration of the proposed connection is depicted in Figure 13 below.

The absorption and scattering cross-sections of Nitrogen (N14) and sodium was evaluated using JANIS from Nuclear Energy Agency (NEA). Figures 14 and 15 present the scattering and capture cross-sections for sodium (Na-23), helium (He-3) and nitrogen (N-14).
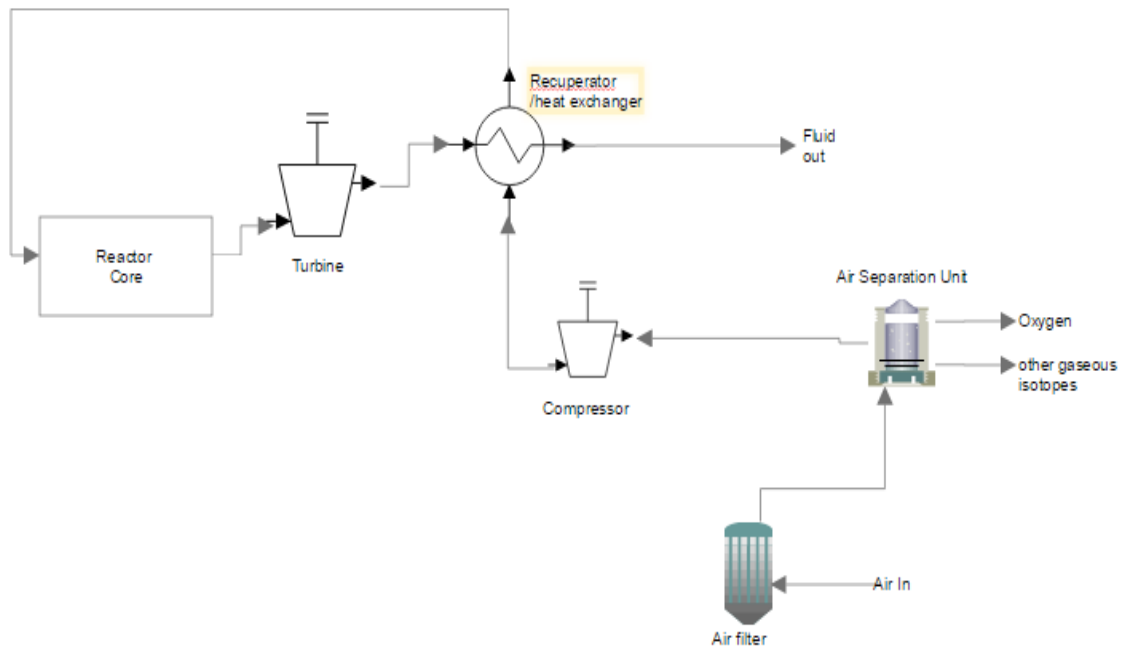
Figure 13. Complete Unit with Nitrogen Recuperation from Air.
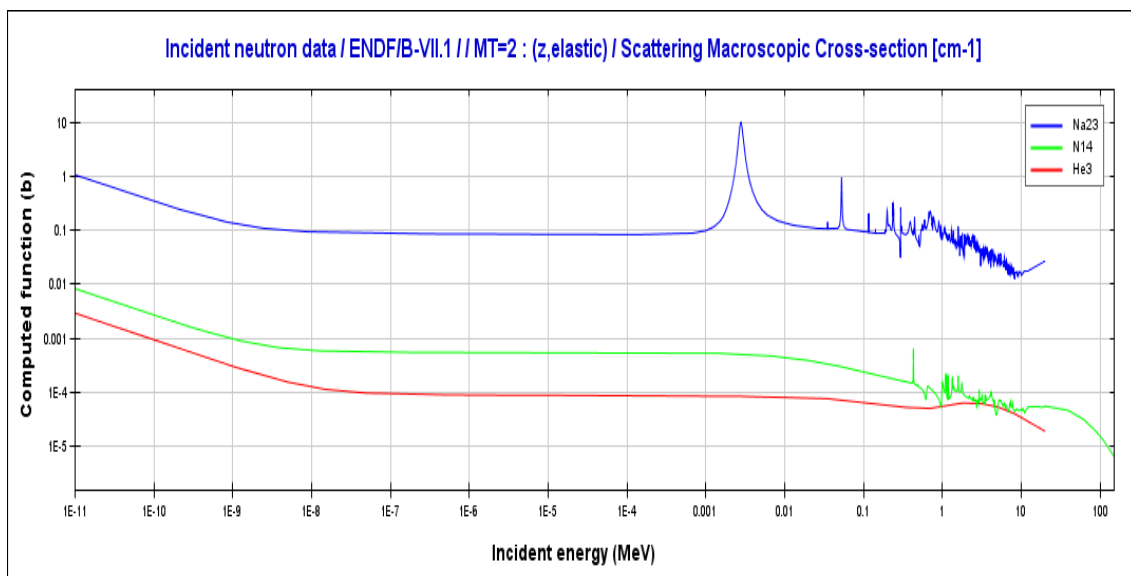
Figure 14. Scattering Cross-Section of Coolant.
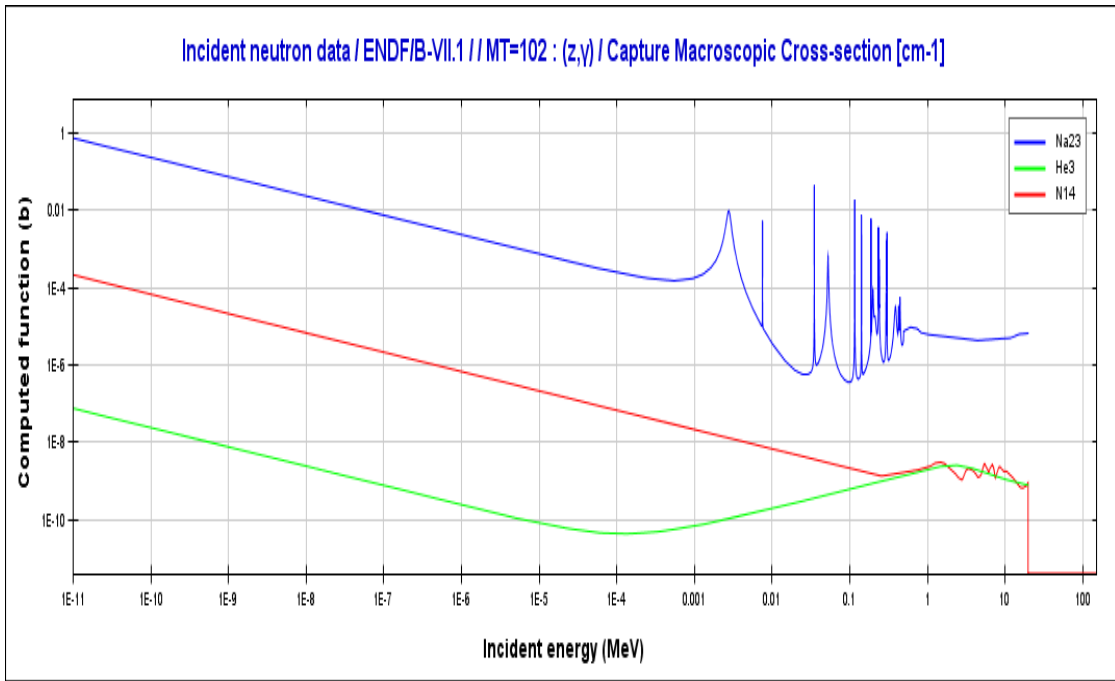
Figure 15. Capture Cross-Section of Coolant.
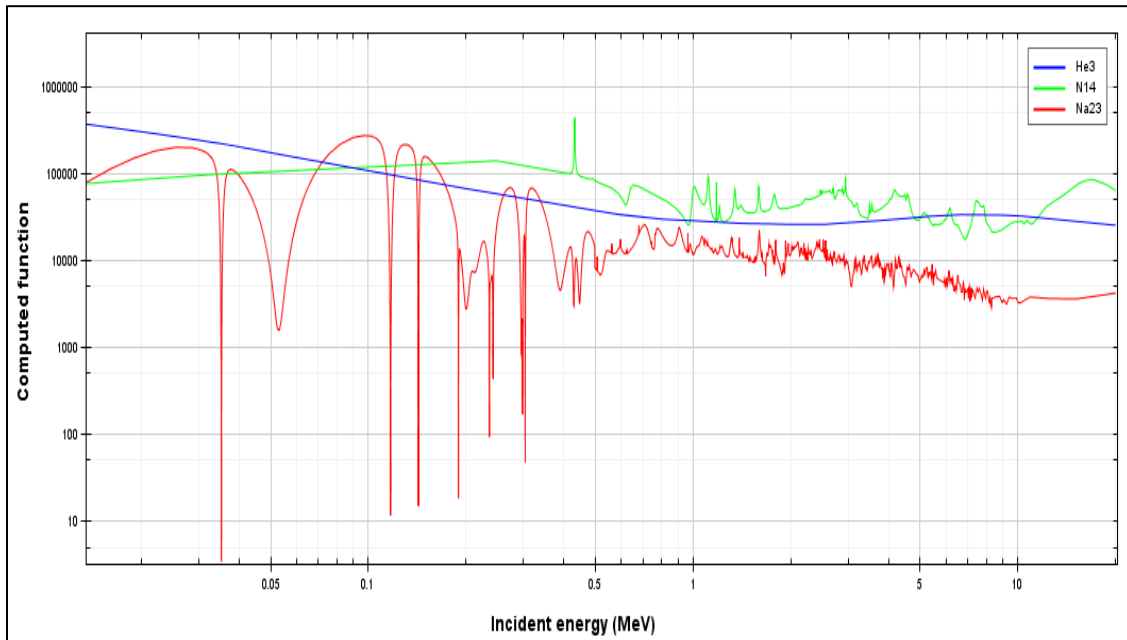
Figure 16. Scattering to Capture Cross-Section Ratio for Coolant Materials.

Figure 15 presents the dominance of sodium in term of neutron scattering. The macroscopic cross-section of sodium is significantly larger (orders of magnitude high) compared to nitrogen and helium. Nitrogen has a better scattering cross-section than helium in both the thermal and fast energy region. Helium exhibits the smallest capture cross-section compared to nitrogen and sodium. The competiveness of nitrogen is exemplified with a plot of the ratio of the scattering to absorption cross-section. The computation of the absorption cross-section only includes the capture cross-section; the other reactions contributing the loss mechanism were ignored because of their small impact, from their small magnitude. This ratio is presented in Figure 16. Nitrogen coolant appears to be very competitive compared to helium and sodium. This ratio appears to be higher than that of helium in the fast energy region.

A comparison of pure nitrogen and air was performed to further demonstrate its appropriateness as a substitute of air. Figures 17 and 18 presents some of the evaluations performed. A system, with configuration presented in Section 5.2.1, was simulated with air and nitrogen to evaluate the energy spectrum and criticality of the system. Figure 17 presents a similar neutron spectrum using both coolants. There is indeed a dominance of fast neutron in both systems.

The system criticality was also evaluated to determine if both coolants will allow the system to consume fuel at a similar or different rate. The results presented in Figure 18, clearly outlines a major similarity between criticality constant per cycle length.
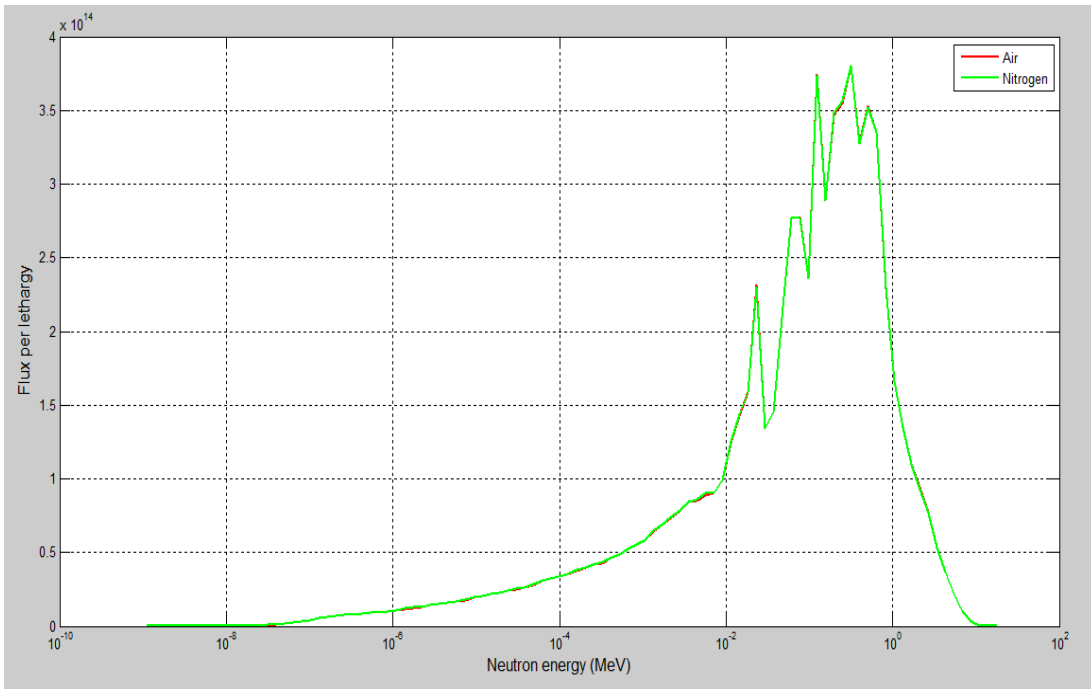
Figure 17. Spectrum Evaluation for Both Coolant Types.
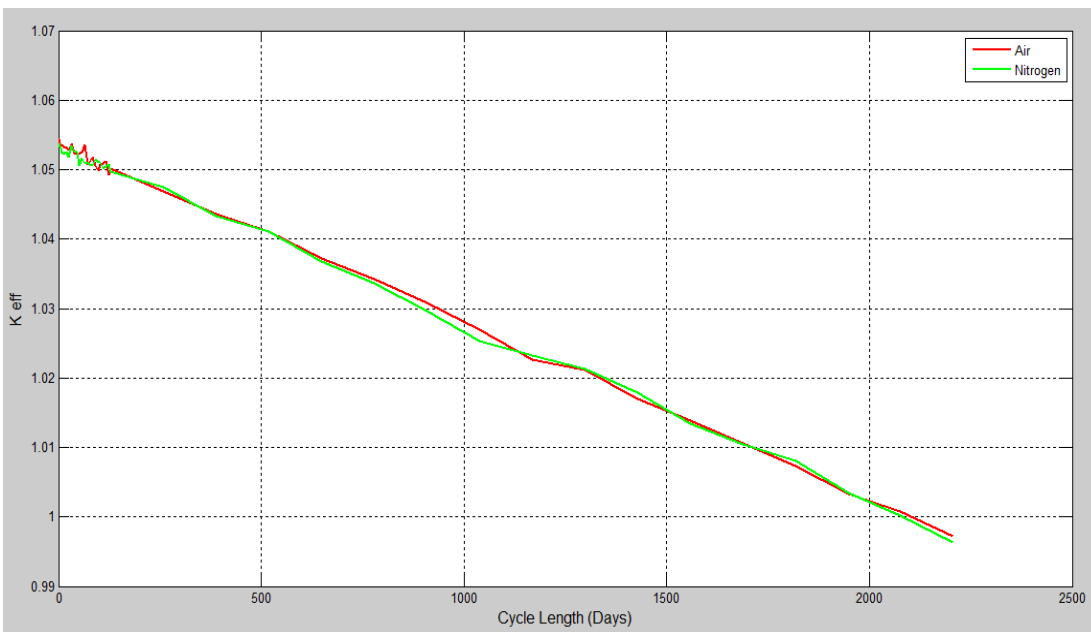
Figure 18. Criticality Comparison Between the Two Coolant Types.

5. REACTOR CONCEPT DEVELOPMENT

5.1 Reference Designs and System Overview

The dimensions of the systems used as references for the design of SACRé are presented in this section. These dimensions were selected following a review of existing and conceptual fast small modular reactor. These reference systems are comprised of the ALLEGRO gas fast reactor, and the conceptual breeder & burner reactor (B&BR) by the Korea Advanced Institute of Technology (KAIST) [45]. ALLEGRO is a demonstrated small gas fast reactor developed at CEA France as an alternative to sodium fast reactors [46]. ALLEGRO reactor uses a combination of fuel plates and fuel rods. Table 8 presents some dimensions of the pin assembly of ALLEGRO.

Table 8. ALLEGRO Pin Assembly Dimensions [47].

Total Power (MWth)	600
Full Core Height (cm)	246
Fissile core diameter (cm)	1.12
Power Peaking Factor	1.43
Pin Pitch (cm)	1.1
Pin Diameter (cm)	0.91
Coolant	Helium
Number of Fuel Assemblies	91

Reports on ALLEGRO system do not provide sufficient information necessary to reproduce a similar system. The Breeder & Burner system was reviewed to complement some of the missing information. Table 9 and 10 presents dimensions that contributed to the design of SACRé.

Table 9. KAIST B&BR Conceptual Design Parameters for Fuel Assembly.

Number of fuel pins	127
Pin Diameter (cm)	1.9
Fuel Radius (cm)	0.89
Cladding Thickness (cm)	0.06
Duct Thickness (cm)	0.3
Inter-Assembly Gap	0.25
P/D	1.064
Flat to Flat Distance	23.72
Assembly Pitch	23.97

Table 10. KAIST B&BR Conceptual Design Parameters for Reflector Configuration.

Number of Reflector pins	91
Pin Diameter (cm)	2.32
Cladding Thickness (cm)	0.10
Duct Thickness (cm)	0.3
P/D	1.03
Assembly Pitch (cm)	23.97
Flat to Flat Distance (cm)	23.72
Core Equivalent Radius (cm)	111.16

Both systems have an active core with a top and bottom reflector and shield. SACRé system was designed with similar full core height, fuel amount and total fission power to that of ALLEGRO, and similar structure thickness for the fuel assemblies, reflector and shield bundles. SACRé has a smaller fuel radius and taller active core length compared to ALLEGRO and B&BR. SACRé is designed with a higher number of fuel assemblies compared to ALLEGRO but a similar number of rods per assemblies to the B&BR. The SACRé core layout is different from that of ALLEGRO and B&BR because it is designed to have a central reflector. These parameters allowed for the design of an initial configuration of SACRé.

5.2 SACRé System Physical Dimensions

5.2.1   SACRé Proposed System Composition

A graphical representation of the fuel rod in SACRé system is presented Figure 19. The rod is composed of the fuel (15% enriched) at the center of rod and a clad material around it. There is a very small gap space between the fuel and the clad to accommodate for swellings from high temperature irradiation. This gaps space is 0.1 mm.
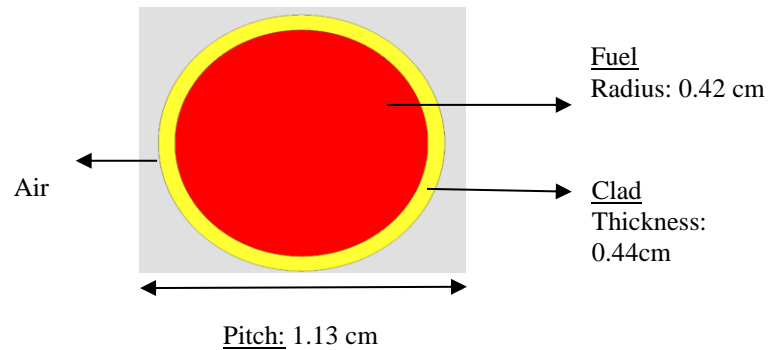
Figure 19. Graphical Representation of SACRé Fuel Rod.

The fuel assembly of SACRé system is composed of fuel rods, a top and bottom reflector and neutron/ photon shield. There are 127 fuel rods in each fuel assembly. The fuel assembly is encapsulated with a HT9 steel. The thickness of the elements composing the fuel assembly is presented in Table 9. The active core of SACRé was design in anticipation of the capacity of air to cool the system with an appropriate mass flow rate. The volume fraction of the fuel and the coolant are presented in Table 11. The proposed design of SACRé active core was evaluated and adjusted from an initial configuration. This initial configuration (Configuration 1 in Table 11) was designed with adjustments presented in the Section 5.1.

41

The volume of the fuel and the total fission power is conserved but the assembly flat to flat dimension for the fuel assembly, reflector, shield assemblies, and the coolant volume is different.

The low density of air and the lack of researches associated with the ability of air to appropriately cool a super-heated system, lead to the focus of the analysis of the third configuration, with the fuel volume lower than the coolant volume. The fuel to coolant volume fraction is about 40.28% and 45.01% respectively. This configuration has a larger amount of air and pitch to diameter ratio. This configuration was selected for the design of SACRé and the fulfillment of the requirement laid out in this thesis, because it is more likely to produce appropriate thermos-hydraulics parameters: reasonable mass flow rate, pressure gradient and coolant axial temperature.

The fuel, axial reflector and shield dimensions, in the active core are presented in Table 11. Table 12 presents a detailed view of the volume fraction of the active core and major changes made to obtain the dimensions deemed appropriate for the design of SACRé.
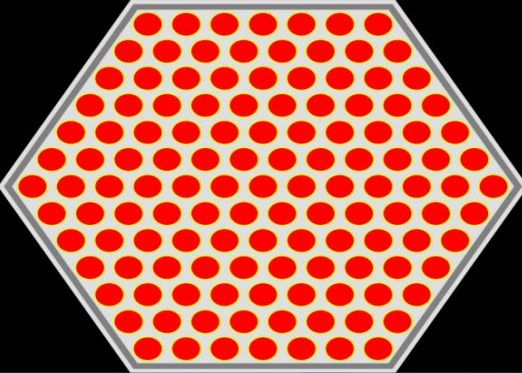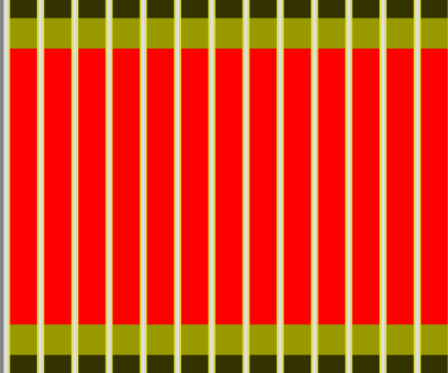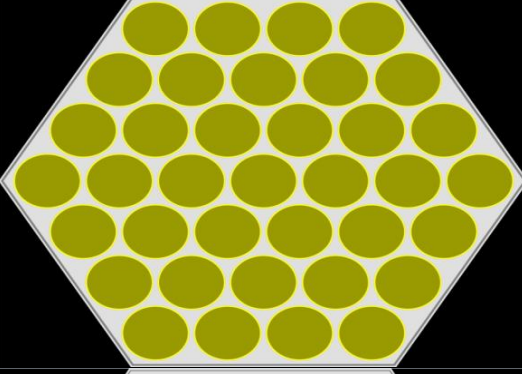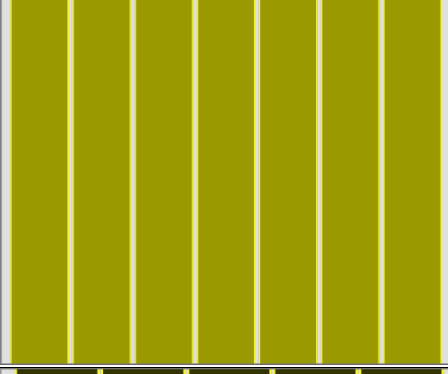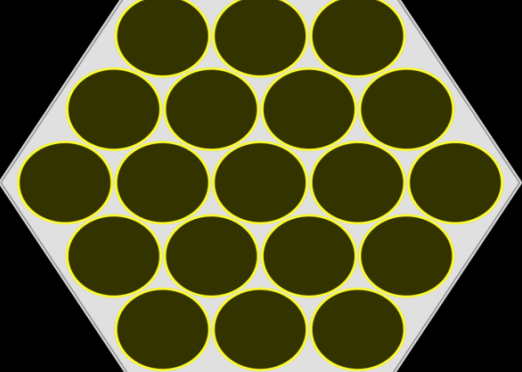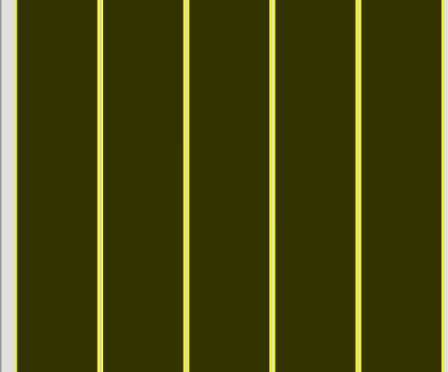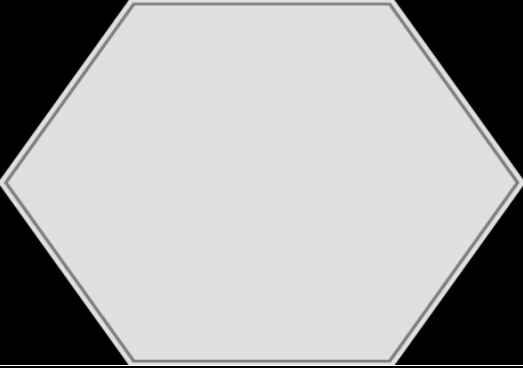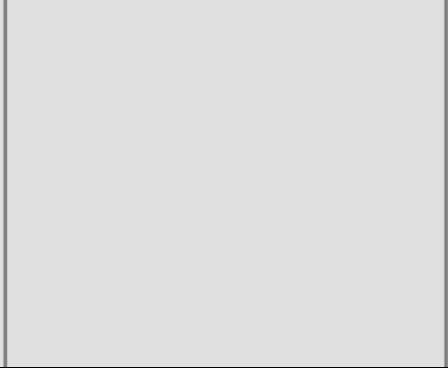
	Radial View	Axial View
Fuel Assembly The fuel is wrapped with clad material. Each rod is manufactured with axial reflectors and shield material. These extra materials are placed on the top and bottom of each individual rod.		
Reflector Each reflector rods are wrapped with a protective agent (clad). The clad material used similar to that of the fuel rods		
Shield Each shield rods are wrapped with a protective agent (clad). The clad material used similar to that of the fuel rods		
Control Rod/Guide Tube The control/guide tube is an empty casing in this case. The element was not modeled and the analysis was performed while accounting for the positive reactivity it will add.		

Figure 20. Graphical Representation of the Reactor Major Constituents

Table 11 Active Core for Configurations.

	Configuration 1	Configuration 2	Configuration 3
	Fuel Assembly		
Assembly Flat to Flat (cm)	15.6	16.2	16.6
Pitch/ Diameter ratio	1.21	1.23	1.24
Fuel Volume Fraction (%)	46.62	42.66	40.28
Coolant Volume Fraction (%)	38.05	42.79	45.01
Structure thickness (cm)	0.3	0.3	0.3
Structure Material	HT9 Steel	HT-9 Steel	HT-9 Steel
	Reflector		
Assembly Flat to Flat (cm)	15.6	16.2	16.8
Structure thickness (cm)	0.3	0.3	0.3
Structure Material	HT9 Steel	HT-9 Steel	HT-9 Steel
Rod Diameter (cm)	0.95	0.95	0.95
Rods per Assembly	37	37	37
Rod Clad Thickness	0.05	0.05	0.05
Reflector Height (cm)	244.3	244.3	244.3
	Shield		
Assembly Flat to Flat (cm)	15.6	16.2	16.8
Structure thickness (cm)	0.3	0.3	0.3
Structure Material	HT9 Steel	HT-9 Steel	HT-9 Steel
Rod Diameter (cm)	1.35	1.35	1.35
Rods per Assembly	19	19	19
Rod Clad Thickness	0.05	0.05	0.05
Shield Material Height (cm)	244.3	244.3	244.3
	Reactor		
Flat to Flat Distance (cm)	200.6	202.8	204.6
Reactor Height	246	246	246
Structure Material	HT9 Steel	HT-9 Steel	HT-9 Steel

Table 12. SACRé Active Core Volume Fraction (Third Configuration).

	Volume Faction
Fuel	40.28%
Coolant	45.01%
Void	0.0002%
Reflector	7.58%
Shield	4.93%
Clad	0.37%
casing/structural material	5.36%

.

SACRé neutron reflector is composed of 37 reflector rods. Each of these rods is wrapped with a cladding material. The reflector bundle is encapsulated in HT9 steel hexagonal structure. The dimensions of the reflector rod and bundle are presented in Table 11. The reflector dimensions for the three configurations were modified to a similar flat to flat distance of the fuel assembly. This modification was done for each configuration.

The neutron shields in SACRé sole purpose is to limit or restrain radiation from leaking out of the system. Some leakages are expected to occur in the system; this is an inherent attribute to most fast reactors. The shield bundle is composed of 19 rods, all wrapped with a casing material (APMT steel). The dimensions of the bundles are presented in Table 11. The shield dimensions was also modified to accordingly.

The control rod/ guide tube in this design consist of a hexagonal tube filled with air. In reality, during normal operation of the reactor, this tube will be filled with some neutron absorber material that will regulate the neutron population of the reactor to maintain the criticality of the system over time. The control rod material will not be implemented in the design of the SACRé. The system will be design in a way that will accommodate the presence and insertion of these negative reactivity materials.

The guide tube will have an arbitrary location in the system central location in the reactor. The guide tube will be an empty tube where utilities or research facilities can conduct some experiment. The design evaluated for the reflector incorporation in this thesis does not include a central guide tube. The difference between having a central guide tube or central reflector will be evaluated with the selected reflector material.

5.2.2 Full Core Analysis

The design adopted for SACRé system is radially and axially presented in Figure 21 and Figure 22 respectively. The system is designed with 108 fuel assemblies with two separate

arrangement of reflector configuration (central and outer). The central reflector is an optional element in SACRé system. The region it occupies can be substitute with a guide tube depending on the needs of the research/utility facility. The difference between including this central assembly rod and using a reflector will be evaluated in Section 5.5.3. The system is designed with a large amount of reflector in the system. The proposed system contains about 217 reflectors. Their main purpose is to limit the leakage rate in the system. The shield rod bundles are located at the periphery of the reactor. Because of the numerous amount of reflector, it is likely these shield bundles will interact mainly with scattered photons.
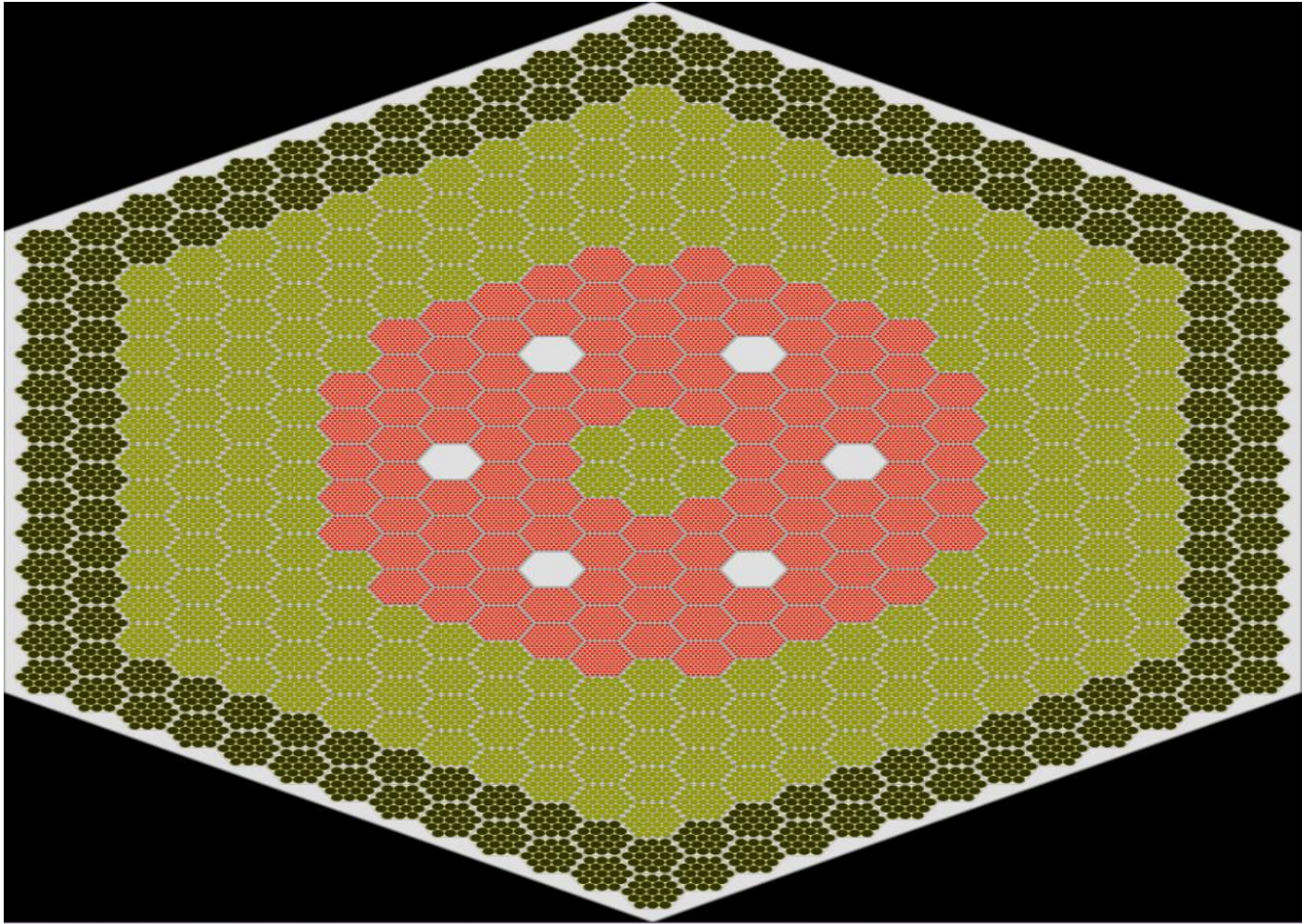
Figure 21. Radial View of SACRé Reactor.
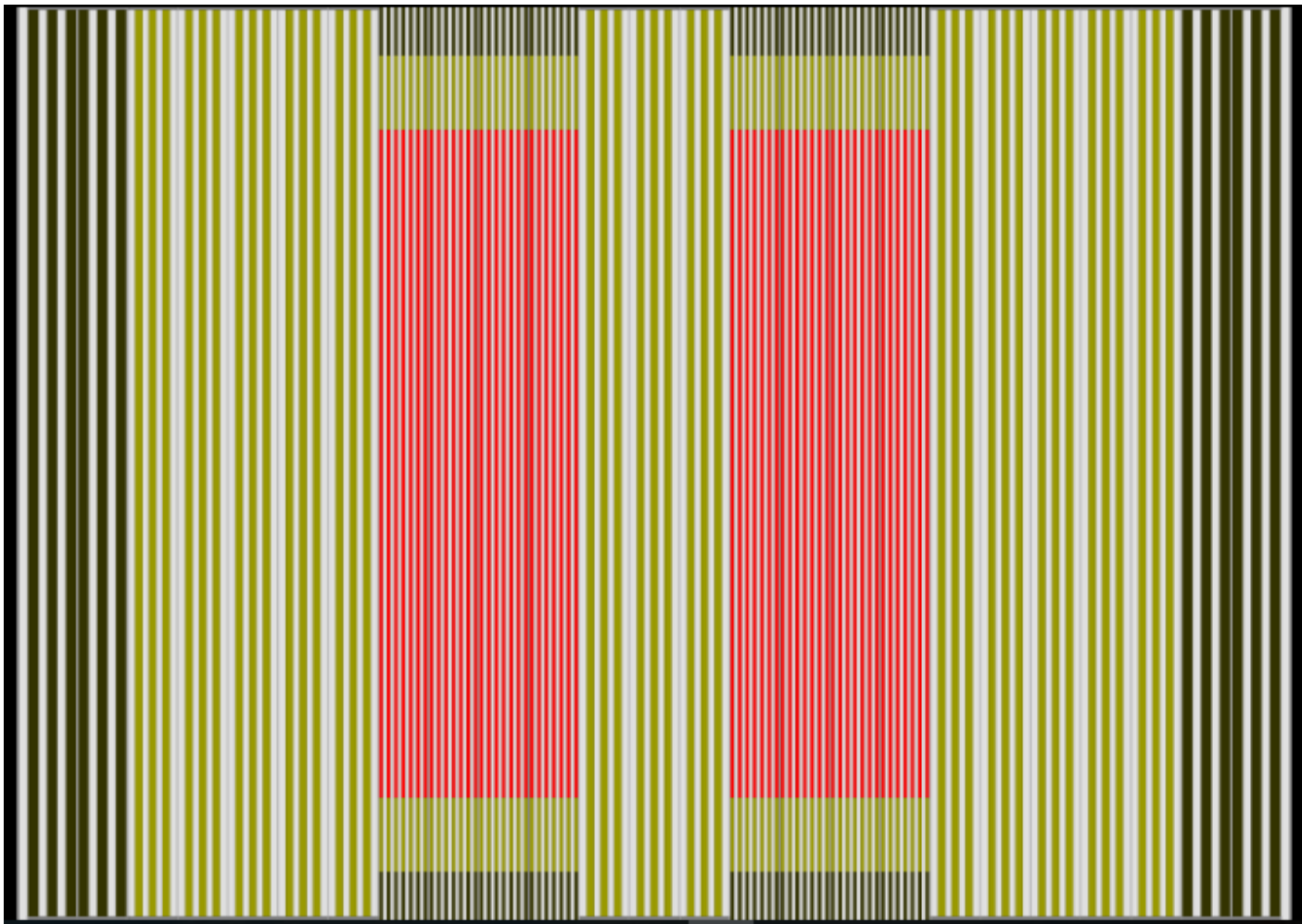
Figure 22. Axial View of SACRé Reactor.

5.3 Fuel Type Selection

The study of different types of fuel and the eventual selection of the fuel type which will be used for the design of SACRé will be evaluated and analyzed with SSS2. For this analysis, three types of fuel including uranium carbide (UC), metallic fuel (U-Zr) and uranium oxide (UO_2) were evaluated and studied. The purpose of this analysis is to determine the fuel type which allows the highest fuel consumption, harder spectrum and long cycle length, for the design of SACRé.

The thermos-physical properties of these type of fuel are presented in Table 13. These fuel types were designed with the dimensions of the rod presented in the previous section to evaluate the flux per lethargy for the fast energy region, from 1E-4 MeV to ~15MeV. The results obtained are presented in Figure 23 and 24. The fuel enrichment for each fuel type, as well as the cladding material.

Table 13. Thermo-physical Properties of the Different Type of Fuel of Interest [48].

	Density [g/cm^3]	Melting Temperature	Thermal conductivity [W/mK]
U-Zr	14	1135 C	14
UC	13.58	2420 C	16.5
UO$_2$	9.72	2865 C	2.9

Figure 24 exposes a pertinent advantage to using metallic fuel in the system as opposed to carbide and oxide fuel. Metallic fuel allows the system to operate for a longer cycle before becoming subcritical. The BOC k_{eff} for an infinitely reflected metallic fuel is 1.24, much higher than that of carbide and oxide fuel.
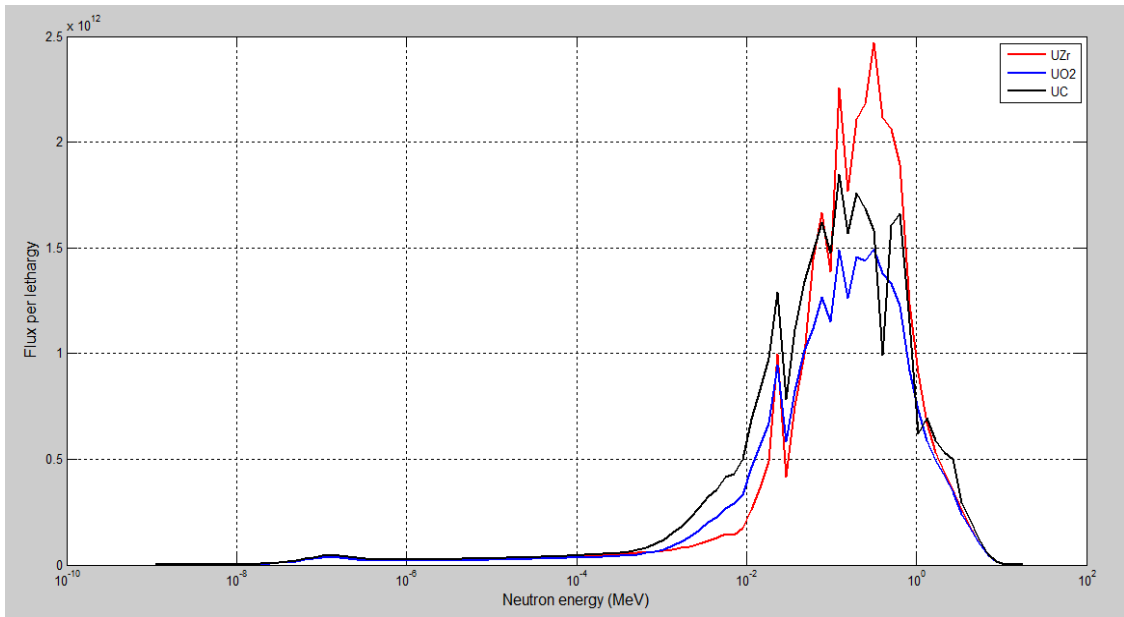
Figure 23. Flux-Lethargy per Energy for Each Fuel Types.

Figure 24. Criticality Evaluation of an Infinitely Reflected Fuel Lattice.

49

Unlike carbide fuel, uranium dioxide fuel is very reputable; it has been extensively studied and tested over years. Oxide fuels have a low thermal conductivity, depraving them from achieving a high similar fraction, with conventional pin configuration. Moreover, oxide fuel has two atoms of oxygen, which consequentially will soften the spectrum. The thermal conductivity of oxide fuel is significantly lower than that of carbide fuel and metallic fuel. This will sequential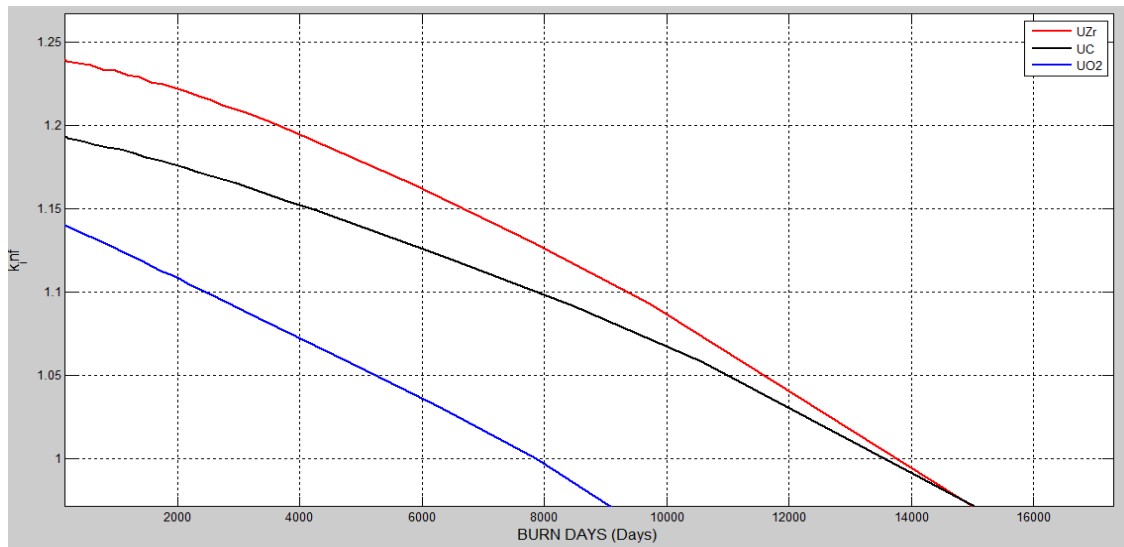ly lead to a higher fuel centerline than that of carbide and metallic fuel at the same power level [49]. The fission gas release, which is increasing with temperature, is much higher with oxide fuel than in carbide or metal fuel [49]. The theoretical heavy metal density of uranium dioxide is smaller than that of uranium carbide and metallic fuel. Hence for the same fuel volume fraction, oxide fuel will require a higher enrichment to obtain criticality than that needed for carbide and metallic fuel [49].

Metallic fuel (U-Zr in this case) is a commonly used fuel type in fast reactors. These fuels are characterized by a very hard spectrum, which results in a high conversion ratio. Unlike oxide fuels, the density of metallic fuel is significantly higher, thus reactivity is not a limiting factor unless the fuel volume fraction is relatively lower [49]. The hard spectrum produced with metallic fuel does however pose some challenges related to fuel cladding endurance. The thermal conductivity of metallic fuel is much higher than that of oxide fuel and carbide fuel. This advantage of metallic fuel is somewhat offset by the relatively low melting temperature. The melting point of pure uranium metal is about 1135°C. This temperature can be raised by adding other elements to make alloys: chromium, molybdenum, titanium and zirconium. Zirconium has a special property in that it enhances compatibility between fuel and stainless steel cladding [49]. In this study, 90% fuel uranium and 10% zirconium are selected to fuel composition. The metallic fueled core has much higher neutron energy than the carbide and oxide fuel. The harder neutron spectrum of this fuel type yields two different effects. Metallic fueled core tends to have

50

a longer reactivity limited fuel cycle length than the carbide and oxide fuel if loaded with the same heavy metal mass and enrichment. This is in fact due to the higher conversion ratio of the metal fuel.

Based on numeral factors and its advantages to other fuel types, U-Zr fuel was selected for further system analysis and the design of SACRé system.

5.4 Clad Material Analysis

The fuel cladding material serves as a barrier between the coolant and the fuel. This barrier's key purpose is to ensure that potential fission product don't leak into the coolant [50]. Some key design criteria of fuel cladding are transparency to neutrons so that it doesn't absorb neutrons that could be used to induce further fission and high thermal conductivity and low thermal expansion coefficient [28].

As mentioned in the previous section, the proposed cladding materials which exhibit favorable characteristics, that will be evaluated in this thesis are FeCrAl, SiC, 304SS, 310SS, 316LSS, APMT steel and Inconel 718. Their thermo-physical characteristics are presented in Table 4. Comparing these properties from the table, promotes the selection of SiC and stainless steel 316 because of their high melting temperature and high oxidation temperature.

JANIS from the Nuclear Energy Agency was used to evaluate the cross-section of major nuclides from the composition of the reflector materials: Iron (Fe-26), Silicon (Si-28), and Nickel (Ni-28). Figure 26 and 27 presents their scattering, and capture cross-section respectively. These cross-sections were plotted with emphasis on the fast energy region, from 1 keV to 15 MeV. The objective of the cross-section comparison is to ensure that the selected cladding material has high scattering aptitude and low neutron capture ability.
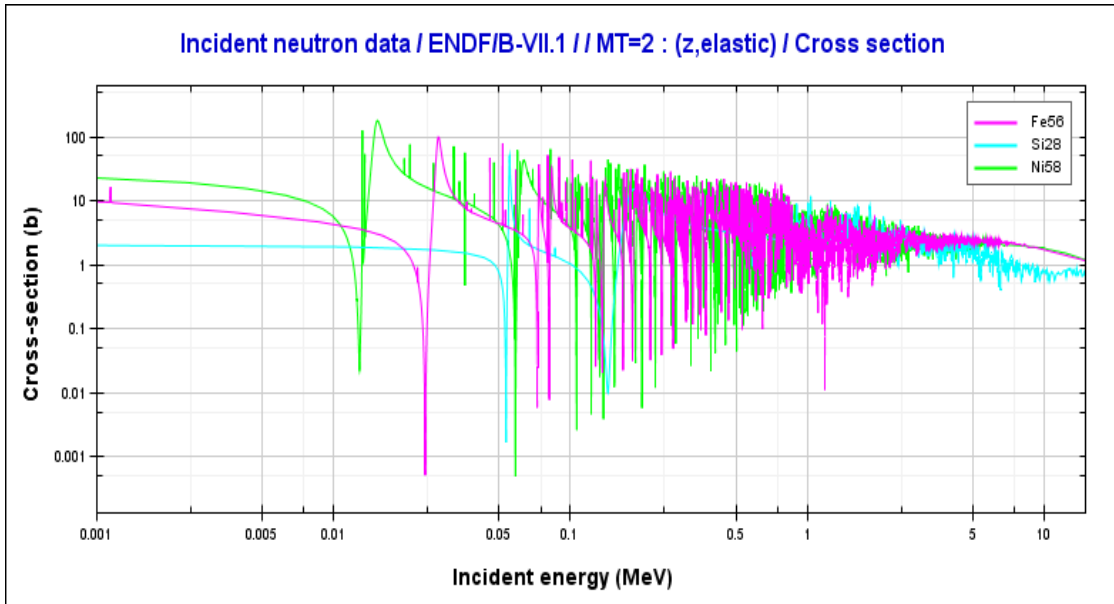
Figure 25. Scattering Cross-Section of Target Cladding Materials.
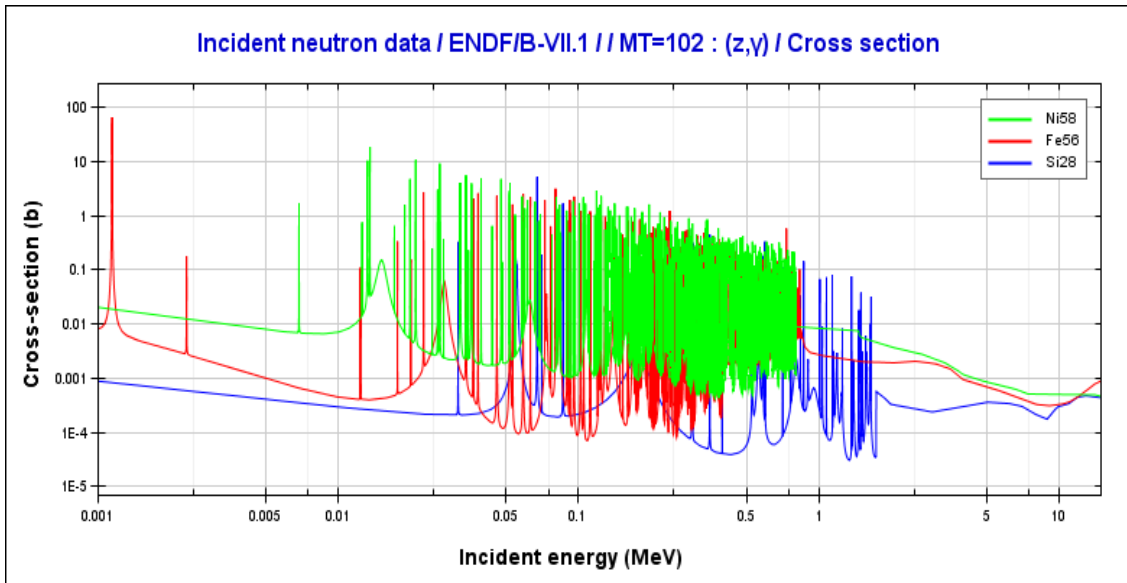
Figure 26. Capture Cross-Section of Target Cladding Materials.

The assessment of the major nuclides from the target cladding material promotes the selection of iron based cladding, notably a material between stainless steel (310SS, 304SS, 316LSS), FeCrAl steel and APMT steel. This selection was made promising because of its relatively low capture cross-section and high scattering cross-section. Silicon (Si-28), despite having the lowest capture cross-section, has the lowest scattering cross-section, which makes it the least attractive material.

An infinitely long and reflected fuel rod was designed to evaluate the neutron spectrum per cladding material. The plots were generated with SSS2 and the results plotted with MTL.A hard spectrum is desired because it exhibits a dominance of high energy neutrons, which is a characteristic of fast reactors.
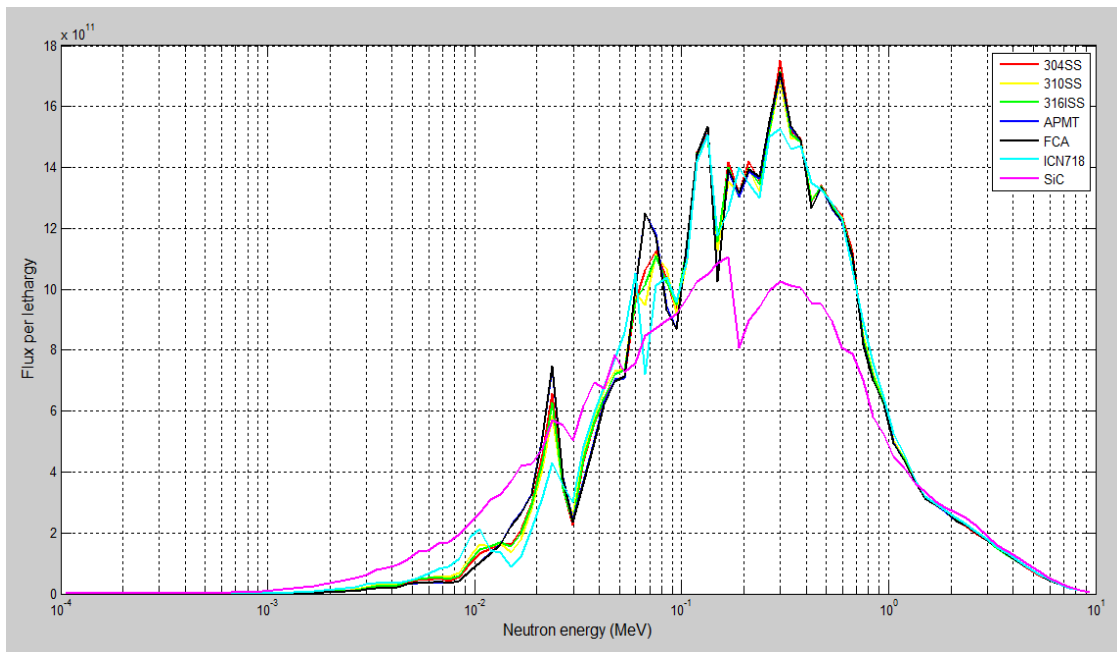
Figure 27. Neutron Flux per Lethargy for Each Cladding material.

APMT steel allows neutron generated from fission in the fuel to travel with high energy. This is demonstrated in Figure 27, with the hardest spectrum. Stainless steel 304 (304SS) also enables a hard neutron spectrum.

APMT will be selected as the fuel cladding not only because of high melting and oxidation temperature but also because it has the highest amount of chromium (Cr) which is a good agent in ensuring a long oxidation in the system during operation.

APMT material will be used to wrap the reflector materials. The transparency of the clad material will not only allow neutrons to interact with the reflecting material to be reflected, but also to protect the material from oxygen and limit the rate of oxidation in the system.

5.5 Reflector Integration

5.5.1 Cross-Section Analysis

Six reflectors were selected to be evaluated and incorporated in the design of SACRé reactor: lead (Pb), lead-oxide (PbO), magnesium oxide (MgO), lead bismuth eutectic (LBE), aluminum oxide (Al_2O_3) and spinel ($MgAl_2O_4$). The thermos-physical properties of these materials are presented in Table 5 in Section 4.4.2.

Neutron reflectors are regions of unfueled materials surrounding the core. Their main function is to scatter neutrons that leak from the core, thereby returning a large fraction of them back into the core. Reflectors "smooth out" the power density by utilizing neutrons that would otherwise leak out from fission within the fuel [51]. The cross-section of the proposed reflector materials are presented in Figure 28 and 29. The plots of the macroscopic cross-section are generated from JANIS, for the nuclide that contributes largely in each reflector materials. These nuclides are lead (Pb-208), magnesium (Mg-24), aluminum (Al-27) and oxygen (O-16).
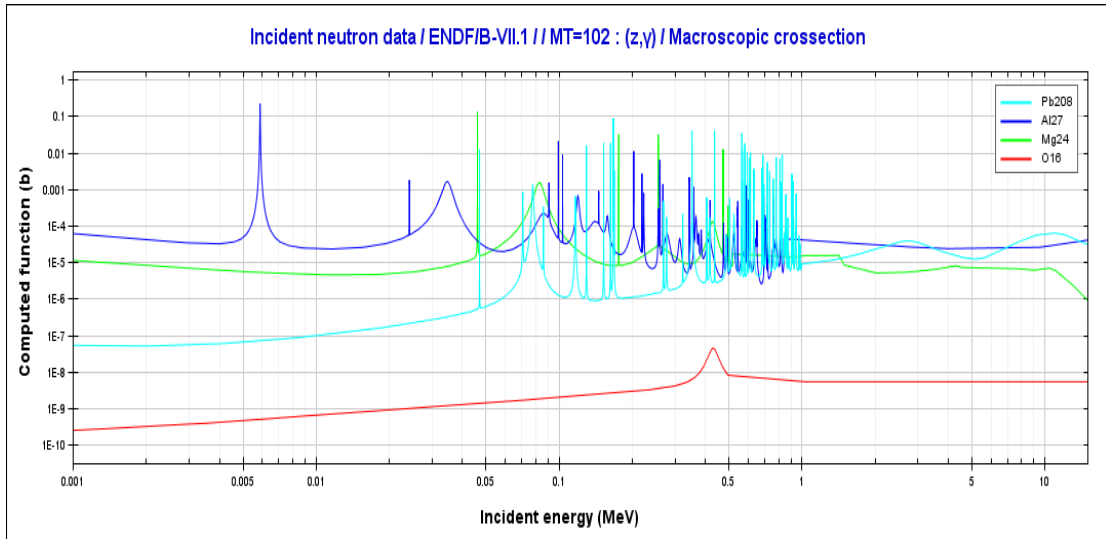
Figure 28. Reflector Capture Macroscopic Cross-Section.
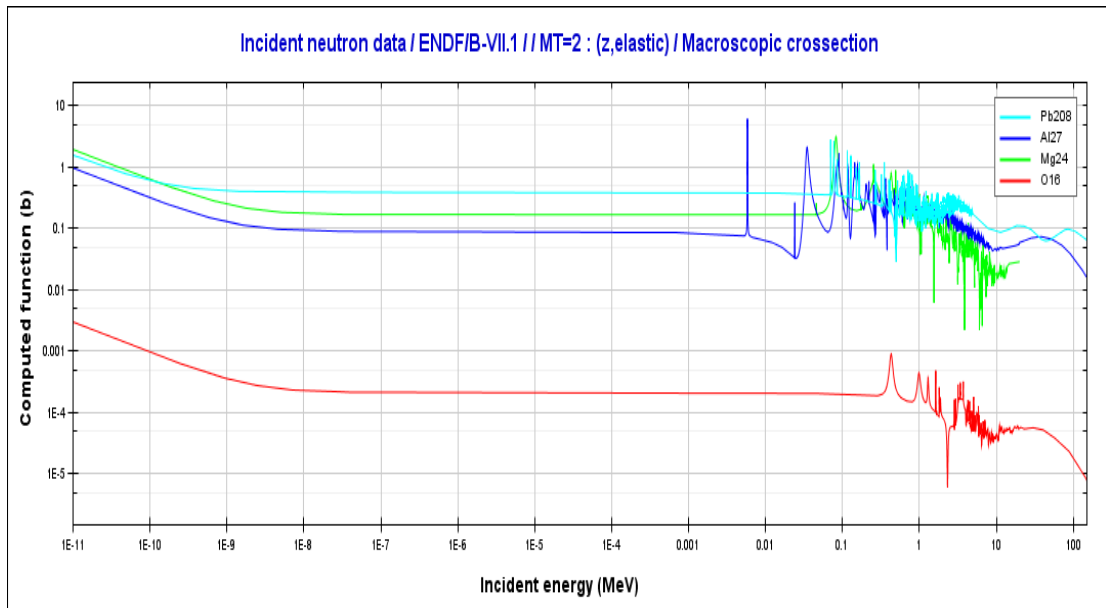
Figure 29. Reflector Scattering Macroscopic Cross-Section.

Having oxygen as major isotopes in a reflector material would not be economical in a rich neutron environment. Despite having the lowest capture macroscopic cross-section, in orders of magnitude, oxygen (O-16) also has the lowest scattering cross-section. Magnesium, lead and aluminum are competitive reflector materials. Aluminum (Al-27) has the highest scattering cross-section, followed by lead (Pb-208) and magnesium (Mg-24). The capture cross-section presents the benefits of having magnesium as a reflector. Lead, despite having the highest scattering cross-section, possess the highest capture cross-section. The choice of the appropriate reflector, in terms of cross-section analysis, will be summarized in the ratio of scatting to capture ratio. An appropriate neutron reflector is defined with a high a neutron scattering ability and a low capture cross-section. A plot of this ratio for each reflector material is presented in Figure 30.
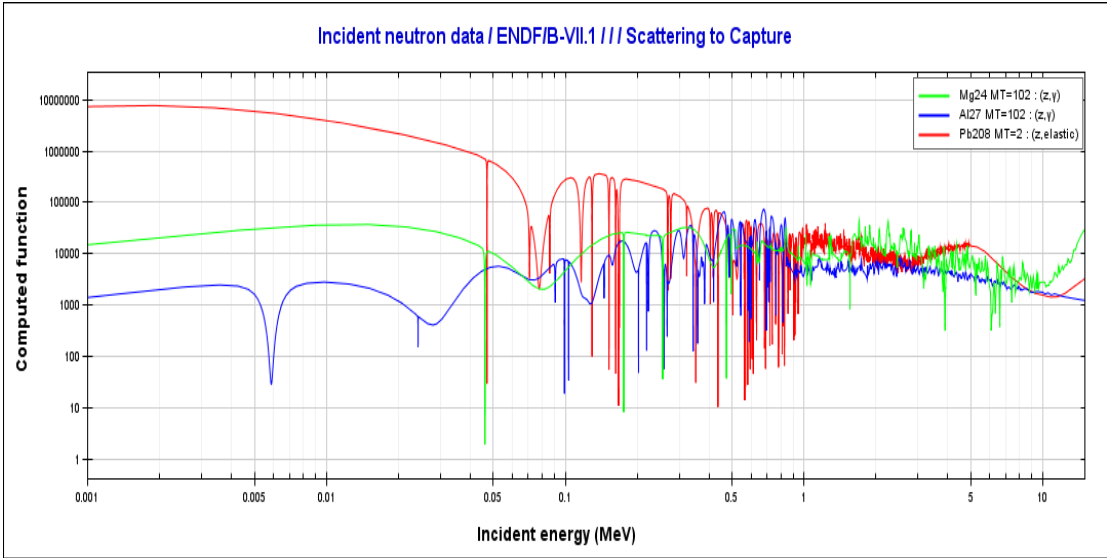
Figure 30. Ratio of Scattering to Capture Cross-section for Each Reflector Material.

SACRé nuclear reactor is a system that operates in the high energy region. The scattering to capture cross-section ratio is competitive for magnesium, lead and aluminum based reflectors. This ratio is on average higher with lead based reflectors followed by magnesium then aluminum based reflectors. Aluminum based reflector is not far off the other two reflectors. Despite having the lowest ratio of the three, its benefits in the system still leaves something to be desired in the design of SACRé.

5.5.2   Neutron Spectrum

SACRé system was evaluated with SERPENT to observe the neutron spectrum in the fast energy region. That region of interest is defined within the bounds of [10 keV – 15 MeV]. This spectrum was evaluated with all the proposed reflector materials. The spectrums observed are presented in Figure 32. Another spectrum was generated for all energy range to verify and ensure that all neutrons are generated and maintained fast, and that a limited to no neutrons are being thermalized in the system. The simulated spectrum is presented in Figure 31. The axial and radial reflector combination were made similar and the system was designed without the gas plenum because this variable doesn't have any direct effect on the neutronics of the system.

Figure 31 and 32 present the ability of the system to generate and maintain neutrons at high energy. These figures also expose the neutron spectrum softness aptitude of the magnesium based reflectors and aluminum reflectors: MgO, $MgAl_2O_4$ and Al_2O_3. Lead (Pb) and lead bismuth eutectic (LBE) allow neutrons generated from fuel to travel at high energy and be reflected with the least amount of energy lost. This phenomenon is as expected; Mg and Al both have a z-value of 12 and 13 respectively and Pb is 82. From conservation of energy and momentum, the energy transfer with low z-material is higher than that of high z values, thus the harder fast region spectrum with interaction of neutron with high z materials as presented in Figure 31 and Figure 32.

57
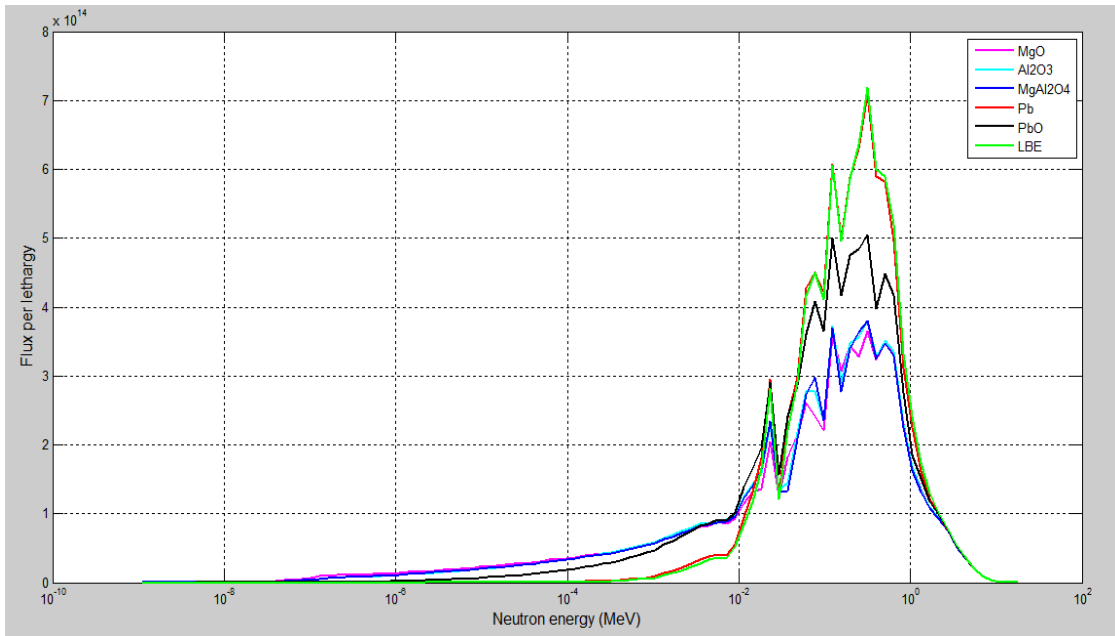
Figure 31. Neutron Spectrum per Reflector Material.
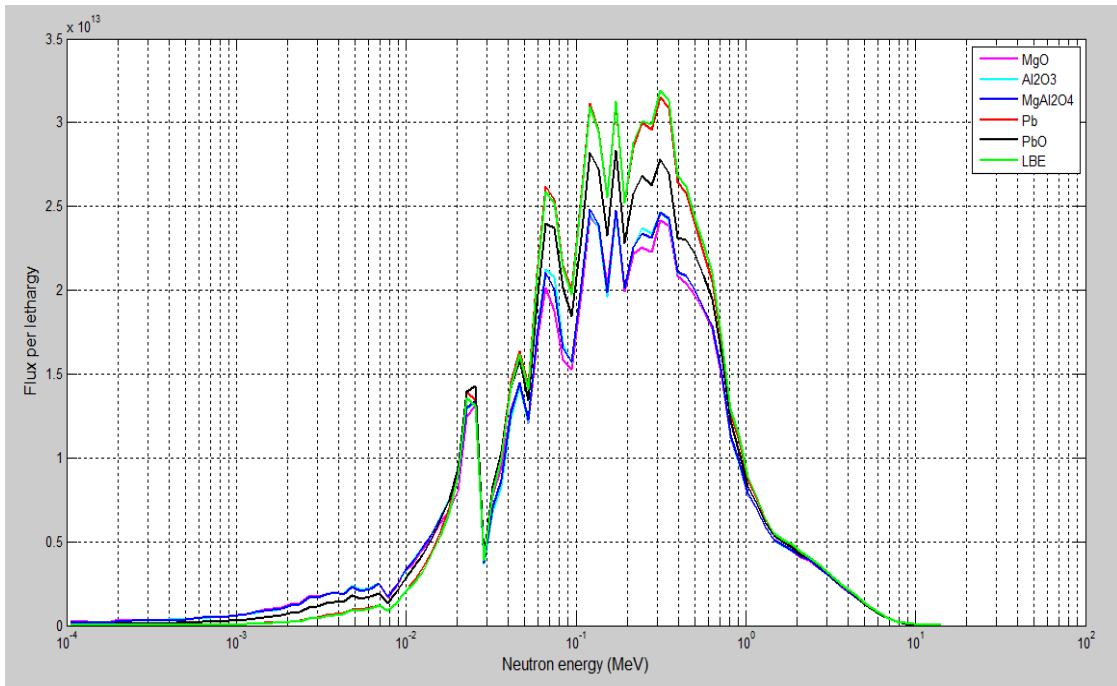
Figure 32. Neutron Spectrum per Reflector Materials for Fast Energy.

5.5.3 **System Performance Characteristics**

SACRé system criticality was evaluated with all the six different reflectors. This analysis was performed to evaluate the cycle length of the system; the time to which the system will require reloading given the small amount of reactivity left in the system. The simulated criticality with each reflector is presented in Figure 33. MgO, Al_2O_3 and $MgAl_2O_4$ presents a high amount of excess reactivity at beginning of cycle (BOC), with an effective neutron multiplication factor (k_{eff}) of 1.0587, 1.0546 and 1.0539 respectively. Despite having a high amount of excess reactivity in the beginning of cycle, the fuel consumption with these reflectors appears higher than that with lead based reflectors (Pb, PbO and LBE). The system cycle length for these three reflector is observed after a system irradiation time of ~2207 days (~6 years) with a corresponding burnup of 85 MWd/kgU. At this level, the k-eff of the MgO, Al_2O_3 and $MgAl_2O_4$ presents a subcritical system while the lead based reflector still exhibit some excess reactivity. Figure 33 and Table 14 present the ability of lead based reflector to enable the system to run for an even longer period of time. PbO and LBE achieved a cycle length of ~7.1 and ~6.7 years respectively, with a corresponding burnup of 100 and 95 MWd/KgU. Using pure lead enabled the system to run for ~7.3 years with a corresponding burnup of 105 MWd/KgU. The analysis on the k_{eff} clearly provides benefits of using lead based reflectors in regards to neutron economy. The end of cycle is longest with lead based reflectors compared to magnesium and aluminum based reflector.
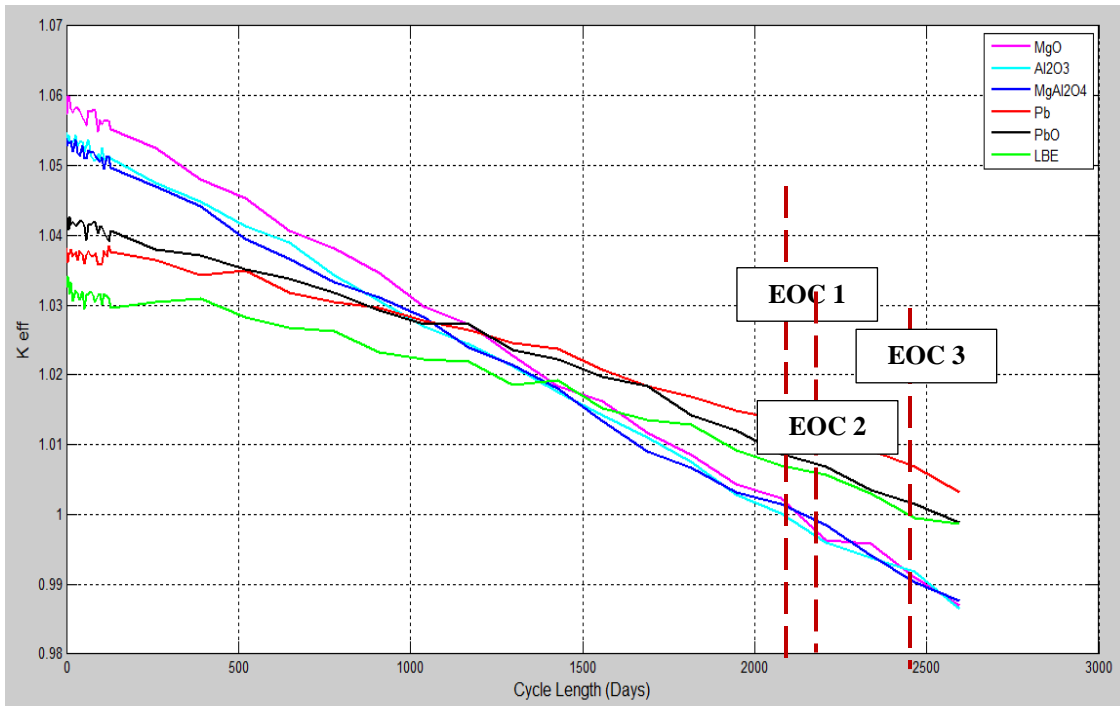
Figure 33. System Criticality per Cycle Length.

Table 14. Comparison of the k$_{eff}$ at BOC and EOC for Each Reflectors.

Reflector Material	BOC K$_{eff}$	EOC 1 K$_{eff}$ 6 years	EOC 2 K$_{eff}$ 6.7 years	EOC 3 K$_{eff}$ 7.1 years	EOC 3 K$_{eff}$ 7.3 years
MgO	1.0587 +/- 0.00051	**0.9963 +/- 0.00062**	-	-	
Al$_2$O$_3$	1.0546 +/- 0.00055	**0.9989 +/- 0.00057**	-	-	
MgAl$_2$O$_4$	1.0539 +/- 0.00059	**0.9985 +/- 0.00064**	-	-	
Pb	1.03807 +/- 0.00060	1.00924 +/- 0.00063	1.00692 +/- 0.00065	1.0032 +/- 0.00065	**0.9989 +/- 0.00057**
PbO	1.04183 +/- 0.00056	1.00350 +/- 0.00059	1.00143 +/- 0.00062	**0.9988 +/- 0.00062**	-
LBE	1.0327 +/- 0.00066	1.00293 +/- 0.00066	**0.9996 +/- 0.00067**	-	-

The effectiveness of the proposed reflectors in this study was evaluated with the analysis of the system's neutron leakage probability. SERPENT simulation provides the non-leakage probability, P_{FNL}. The leakage probability is obtained from the following calculation:

$$P_L = 1 - P_{FNL} \tag{18}$$

Figure 34 presents a variation of the leakage probability per cycle length. Pb and LBE present the highest neutron leakage probability while MgO has the lowest leakage, followed by Al_2O_3 and spinel ($MgAl_2O_4$).

The leakage probability is dominant axially as opposed to radially because of the small thickness and thus a smaller volume of these variables in the core. As presented in Table 10, the axial reflector (both the top and bottom) constitute only 7.58% of the active core and even smaller when compare to the entirety of the core. Figure 34 promotes the selection of magnesium based reflector and Al_2O_3 reflector as opposed to lead based reflector because of the low neutron leakage in the system. The leakage probability of lead based reflector, despite being the highest, is still small since the non-leakage probability is still in the 90 percentile.

The conversion ratio was evaluated with SSS2. The conversion (breeding) ratio is the rate of fuel generation relative to the rate of fuel consumption [52]. The fuel generated evaluated in this system is largely made of Pu-239. The conversion ratio is simulated with SERPENT. This parameter is an important element in all fast reactors; it presents the ability of s system to breed or burn fuel during irradiation. In SACRé system, the conversion ratio should be maintained smaller than 1.0 in the equilibrium core in order to achieve a burner system. The conversion ratio, as presented in Figure 36, is smaller than 1.0 in BOC and gradually increases with burnup until their corresponding EOC. That increment is due to the higher reproduction factor from the breeding of Pu-239. The conversion ratio is higher with lead based reflector and lowest with

MgO reflector. The proposed system is designed to be a burner and not a breeder system. The low conversion ratio observed with Magnesium based reflectors and Aluminum reflector makes them appropriate choice for the design of SACRé.
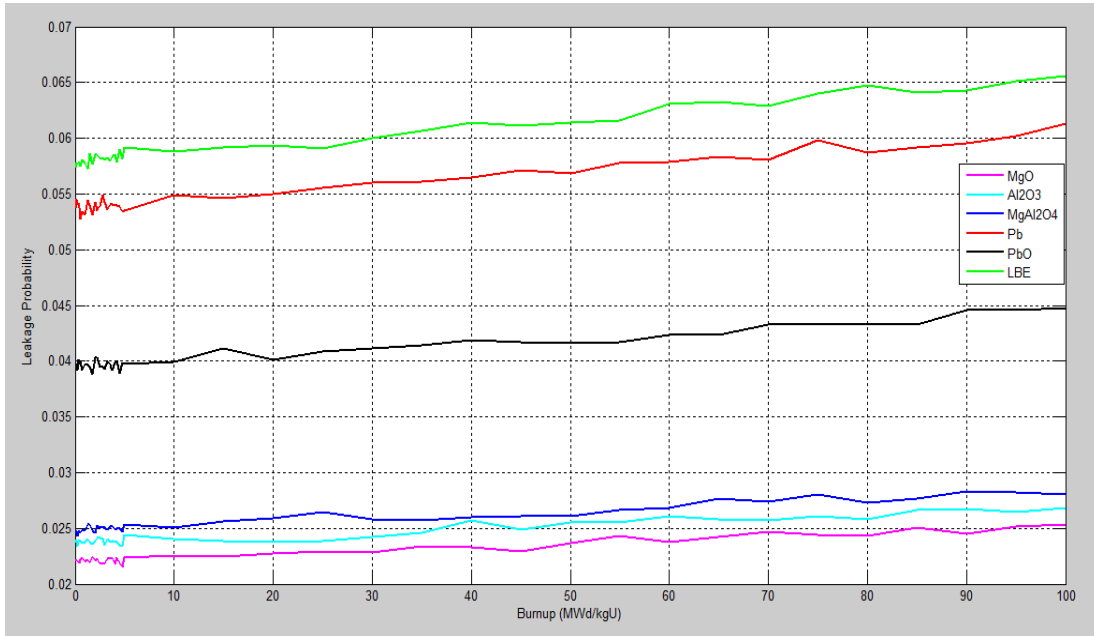
Figure 34. Neutron Leakage Probability for Various Reflector Type.

The illustration of the conversion ratio is detailed with a plot of the fuel consumption and the production of plutonium in the reactor. These elements are presented in Figure 37 and Figure 38. Pu-239 is produced at a higher rate with lead based reflector as opposed to MgO, spinel and Al_2O_3reflectors. This difference is noticeable between the middle of cycle (MOC) and end of cycle (EOC). For a breeder system, the conversion ratio is expected to be at least 1.0 where the rate of production of Pu-239 in the system is significantly higher.
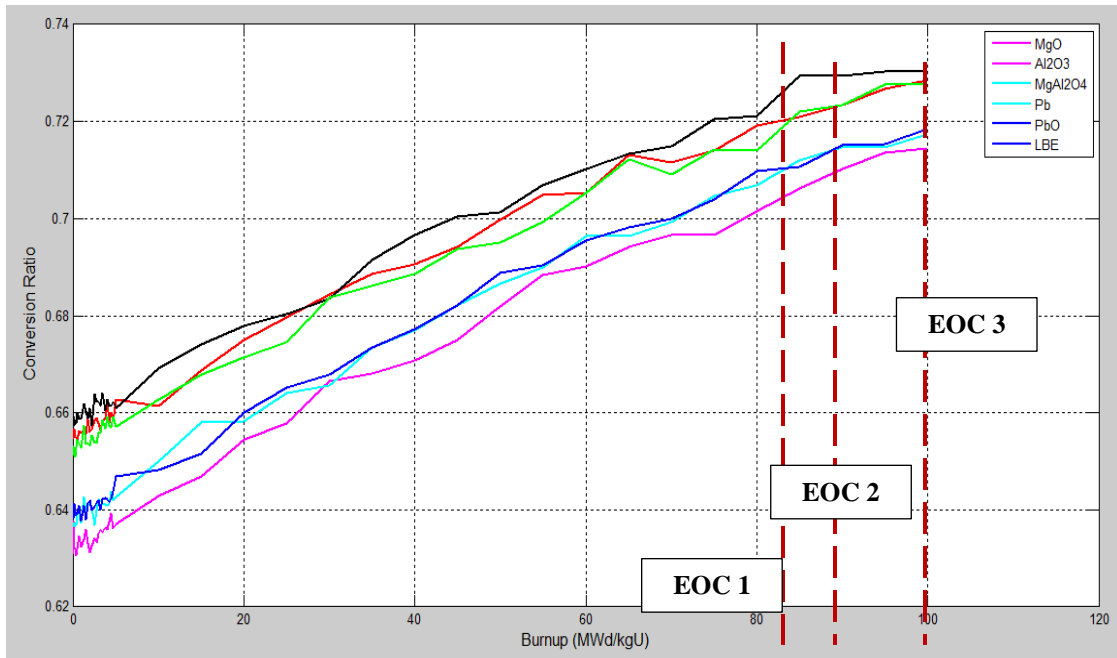
Figure 35. Conversion Ratio per System Burnup.
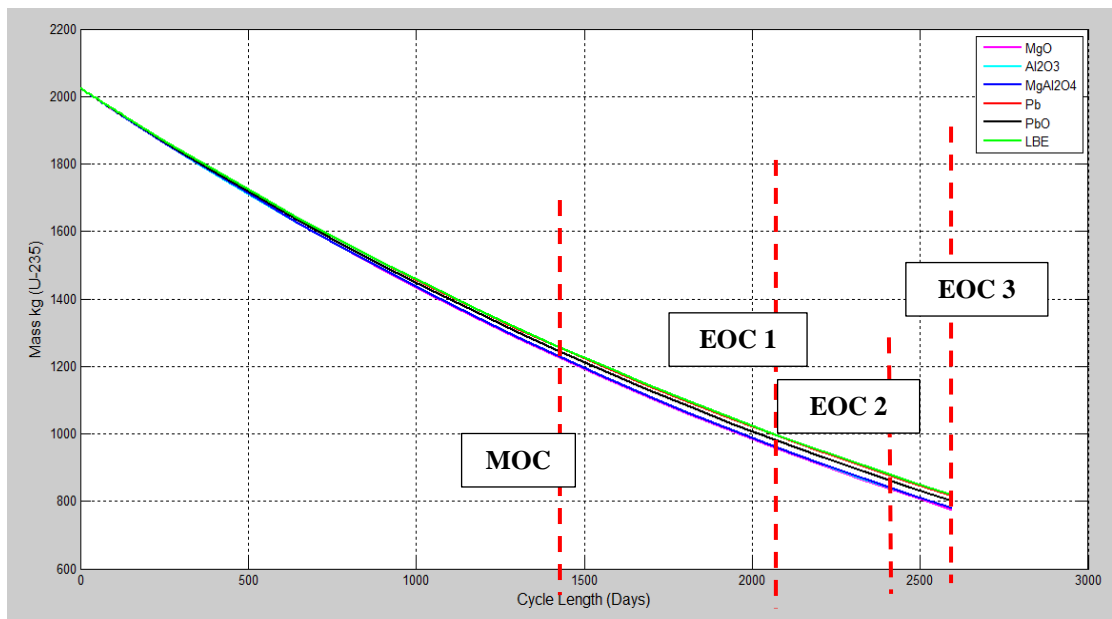
Figure 36. Fuel Consumption per Cycle Length.

63
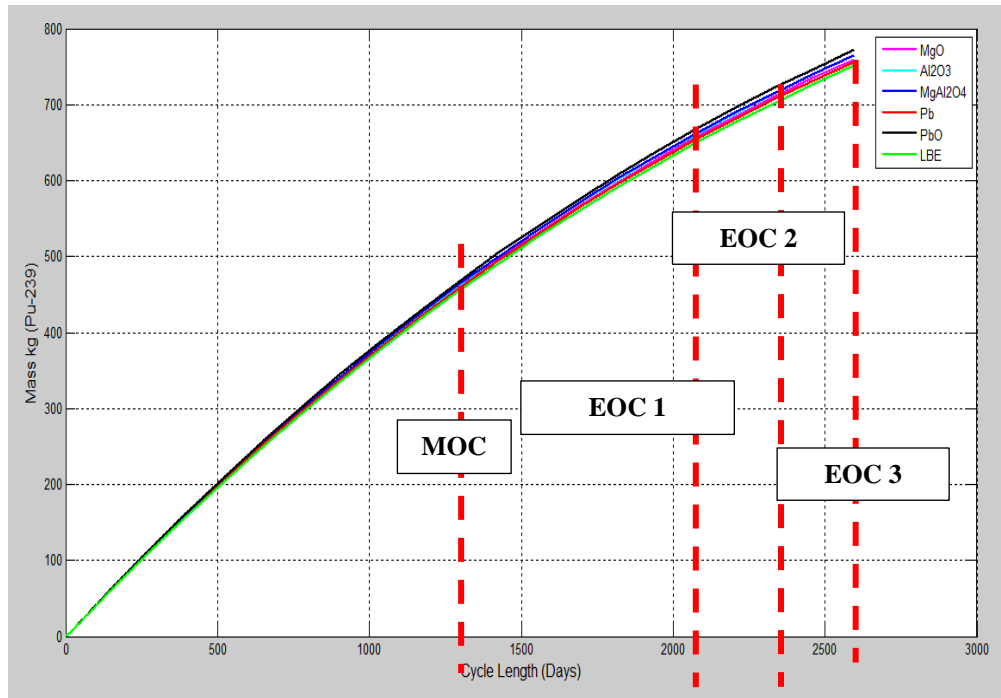
Figure 37. Production of Pu-239 in The System.

The reactor axial flux was evaluated for each of the proposed reflectors materials. This variable was evaluated at BOC and their corresponding EOC, as shown in Figure 38 and 39. All six reflectors show a high peaking flux close to the center of the active core. The plotted fluxes exhibit similar shape. Lead based reflectors, notably LBE and Pb, allow a higher flux close to the center of the core compared to Magnesium based reflectors and Al_2O_3. The axial flux at the end of life shows an increase from the one at beginning of life. The peak seems to have slightly shifted upward, but the new peaking locations are similar with the other reflectors. Figure 39 also presents a decrease in difference between the reflectors. From BOC to their corresponding EOC, the significance of their difference decreased.

64
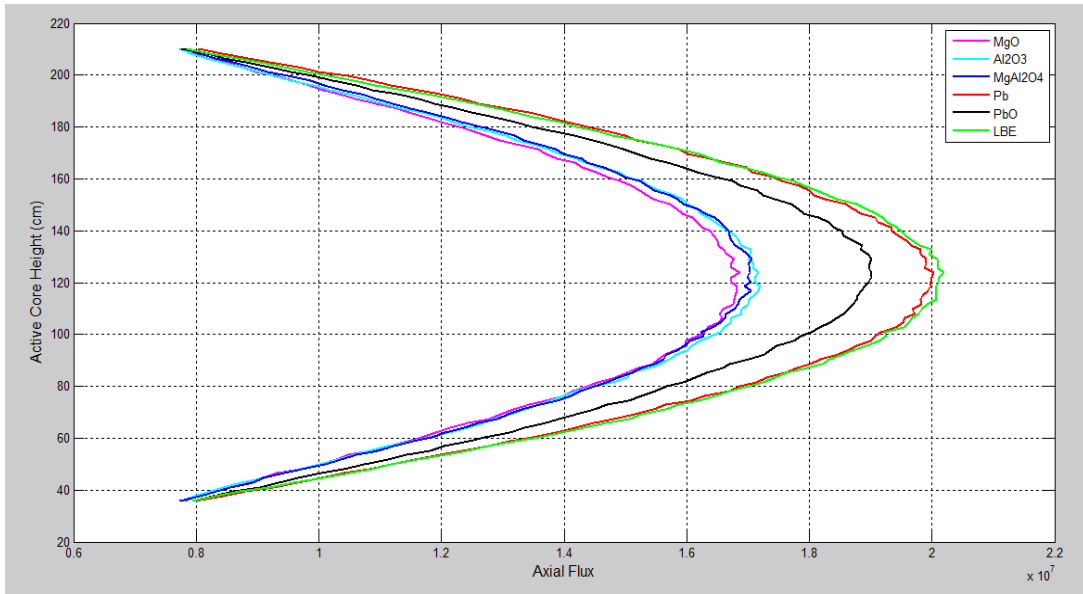
Figure 38. Axial Flux Distribution for Various Cycle Lengths at BOC.
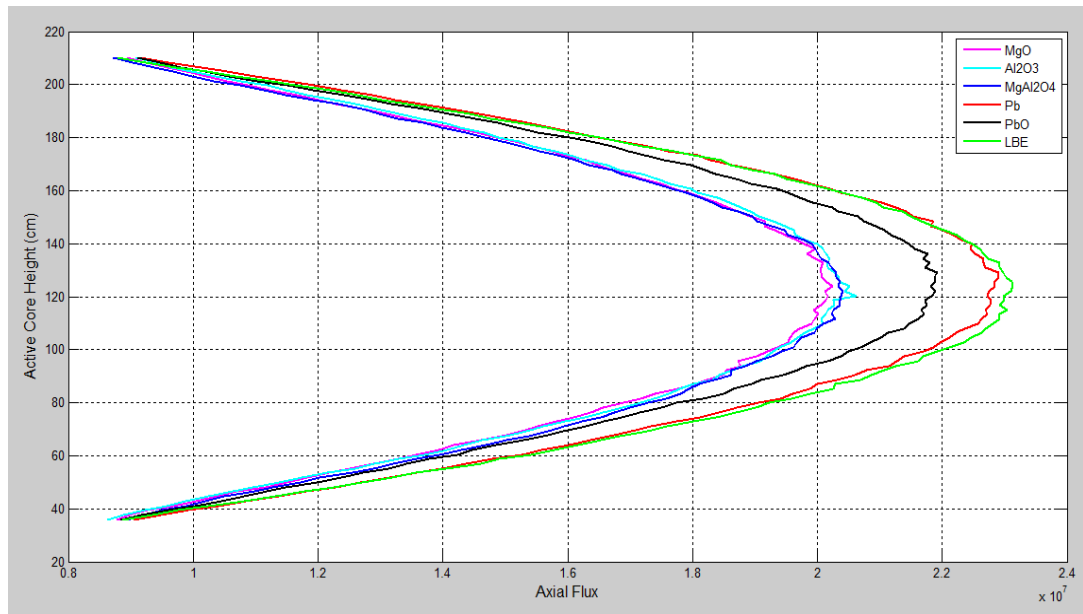
Figure 39. Axial Flux Distribution for Various Reflectors at Their Corresponding EOC.

65

The radial power distribution was evaluated for both beginning of cycle and the corresponding end of cycle for each of the proposed reflector materials. These power profiles are presented in Figure 40 and 41.

The values presented on the color mapping are in units of MWth. All the different reactor designs with different reflector material, present a peaking of the flux around the centralized reflector. The assembly power goes from ~3.5MWth (for LBE reflected reactor) to ~8.5 MWth (MgO). The fuel regions around the centralized reflector have the highest assembly peaking power with MgO, $MgAl_2O_4$ and Al_2O_3reflector and the lowest with the lead based reflector. This different is fairly significant; the percent difference between them is 12.5% in favor of the magnesium based reflector. The radial power distribution for both MgO and $MgAl_2O_4$ reflector appear to be somewhat flat in comparison with the lead based reflectors, from 3rd ring going outward. This is due to aptitude of Mg to soften the spectrum (Figure 32) and enhance the fission rate of the assemblies closed to the reflector. This partial flatness of the radial power is also observed at the end of the cycle. The radial power distribution with lead based reflectors presents a need to further evaluate the core loading to obtain a flat power distribution.

The radial power is expectedly lower at the periphery compared to the center region. The peripheral radial power for lead based reflectors appears to be lower than that of the magnesium based reflector and Al_2O_3 reflector. Neutrons traveling outward, after interacting with lead based reflectors, lose less energy as opposed to magnesium based reflectors. This is because lead is heavier than magnesium. Magnesium oxide reflector, from the analysis performed in the previous sections, will offer the best system performance with a fuel loading enriched to 15%.

.
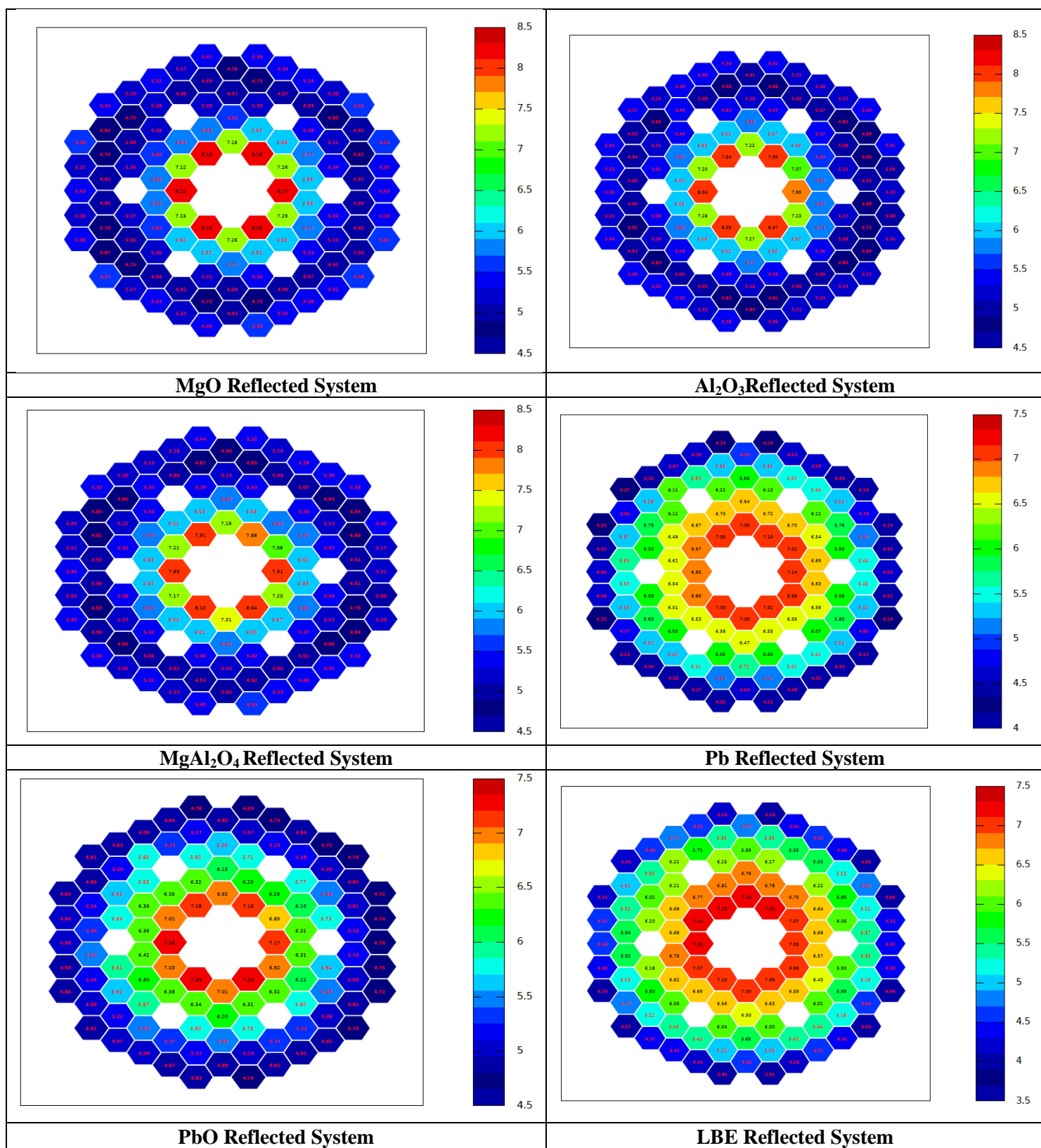
Figure 40. Radial Power Distribution for Various Reflectors at BOC.
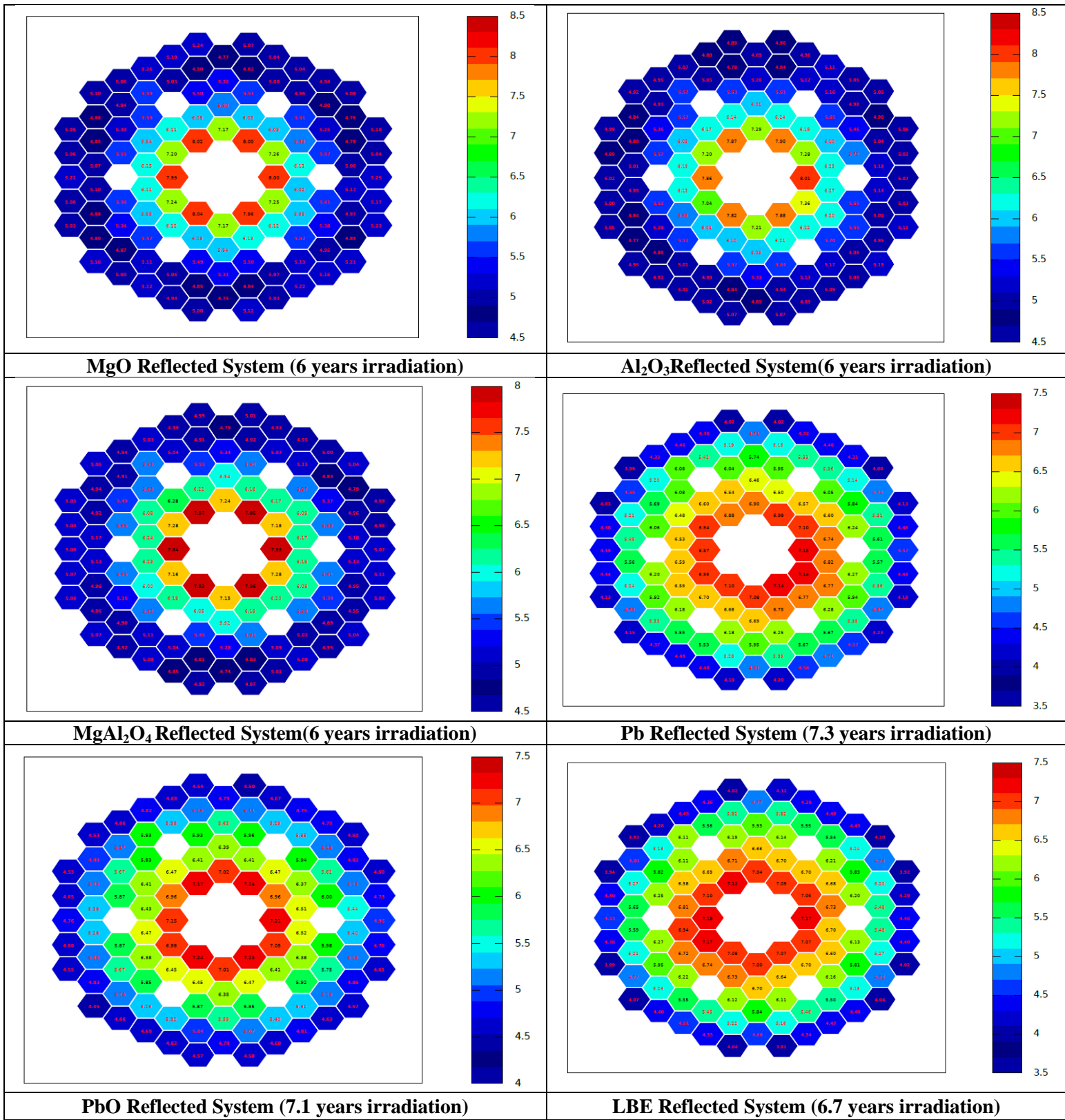
Figure 41. Radial Power Distribution for Various Reflectors at EOC

System with Reflector in Central Region (MgAl2O4)	System with Guide Tube in Central Region (MgAl2O4)
BOC Keff: 1.0539 +/- 0.00059	**BOC Keff:** 1.0528 +/- 0.00059
Conversion Ratio: 0.64	**Conversion Ratio:** 0.64
Cycle length: ~6 years	**Cycle length: ~**6 years

System with Reflector in Central Region (MgO)	System with Guide Tube in Central Region (MgO)
BOC K$_{eff}$: 1.0587 +/- 0.00059	**BOC K$_{eff}$:** 1.0585 +/- 0.00059
Conversion Ratio: 0.63	**Conversion Ratio:** 0.63
Cycle length: ~6 years	**Cycle length: ~**6 years

Figure 42 Central Assembly Analysis.

As introduced in Section 5.1.1, SACRé is intended to be a system win an arbitrary interchangeable central assembly; the region it occupies can be replace for a reflector or a guide tube depending on the need of the utility or research facility. The two proposed arrangements were evaluated to determine if their differences, if any, is significant. This evaluation was performed at BOC for the power and criticality. The simulations were performed with and MgAl$_2$O$_4$ and MgO reflectors. The results obtained are presented in Figure 42.

The difference presented in the above figure is not very significant. Despite having very small difference in power distribution and a criticality constant, the difference between them is about 0.02% and their breeder ratio is the same for both cases.

5.5.4   Assembly Lattice Analysis

A detailed analysis of the assemblies located at the periphery of the core was performed to evaluate the pin power distribution both at beginning of life and end of life. The selected lattice chosen is located at position presented in Figure 43.

Note: Picture oriented to match the orientation of the results.
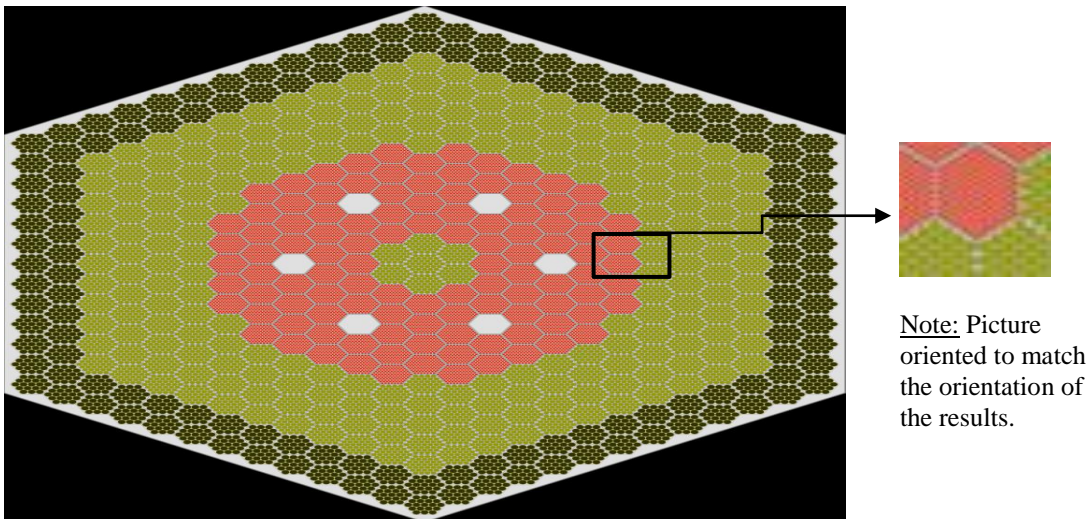
Figure 43. Analyzed Assembly Location.

70

These pin power mappings are presented in Figure 44 and 45 for BOC and corresponding EOC per reflector materials. It is important to note that the right of the analyzed assemblies mark the beginning of the reflector and the left marks the end of the fuel assemblies.

The impact of the softer neutron spectrum from magnesium based reflector is detailed in the presented Figures. Lattice power peaks closer to the reflector than to the fuel assemblies, as opposed to that of the lead based reflectors. Neutrons moving outward, upon interacting with magnesium based reflector, loose energy. They are largely absorbed when returning to the pin. The energy lost is not as significant with lead based reflector as presented in Figure 44 and 45. The power at BOC and corresponding EOC appears somewhat flat in the selected lattice with Al_2O_3 and the magnesium based reflectors. The peaking is highest with the magnesium based reflectors as opposed to the lead based reflectors.
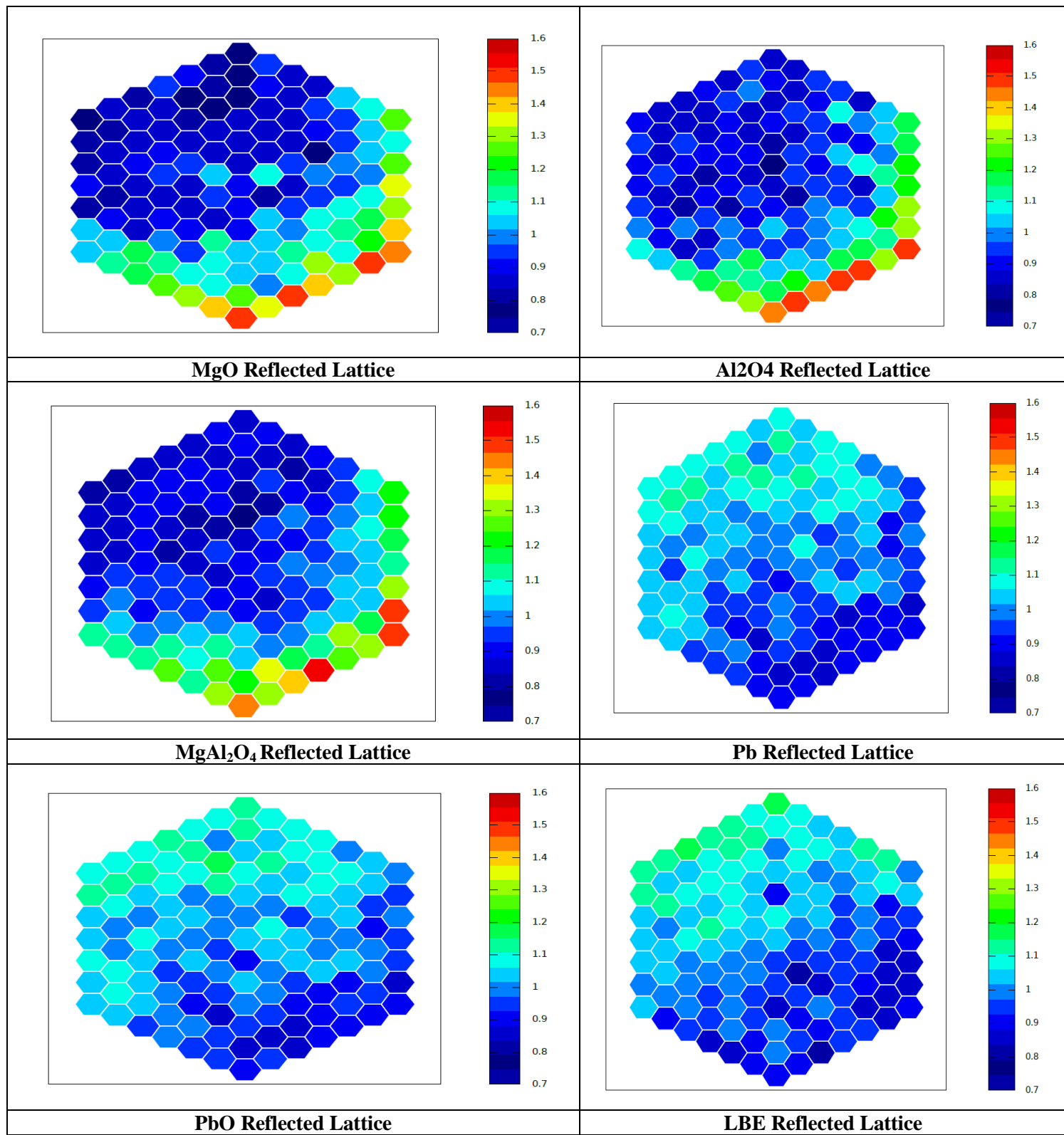
Figure 44. Radial Power Distribution for Pre-selected Lattice at BOC.

The six panels are labeled:

MgO Reflected Lattice

Al2O4 Reflected Lattice

MgAl$_2$O$_4$ Reflected Lattice

Pb Reflected Lattice

PbO Reflected Lattice

LBE Reflected Lattice

MgO Reflected Lattice

Al2O4 Reflected Lattice

MgAl₂O₄ Reflected Lattice

Pb Reflected Lattice

PbO Reflected Lattice

LBE Reflected Lattice
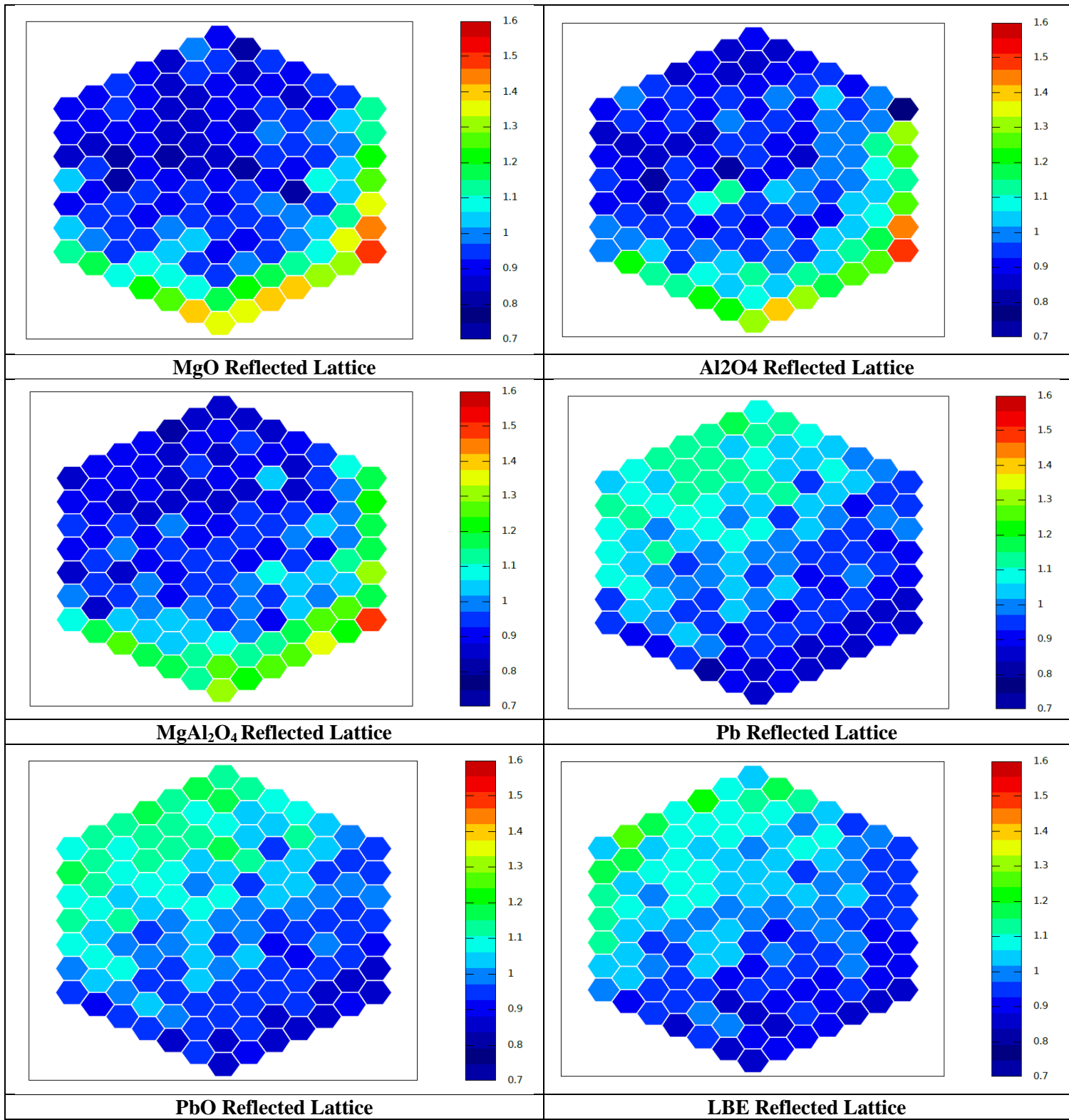
Figure 45. Radial Power Distribution for Pre-selected Lattice at EOC.

6. CONCLUSION

6.1 Summary and Considerations for Material Selection Option

SACRé is a 600MWth rated nuclear reactor modeled in this thesis, with air as a primary and secondary fluid. The proposed system is designed with 108 fuel assemblies, 217 reflectors and 138 shield assemblies. This thesis proposed three different combinations and configurations of the active core, based on the fuel to volume ratio. However, it promotes the third configuration where the fuel volume fraction is smaller than the coolant volume fraction, (40.2% -45.01% respectively). The fuel volume and fission power is conserved but the core diameter and flat to flat distance for all its constituents are modified to account for extra fuel volume. This configuration was estimated as highly favorable because of the low thermal conductivity and density of air, and compared to the other two configurations, it will provide better thermal hydraulics variables, including a reasonable mass flow rate, pressure gradient and appropriate heat transfer configuration. The system was simulated with an estimated fuel temperature at 875°C and coolant temperature at 575°C.

A study of the fuel types, and the reflector and cladding material lead to the selection of a system composed of metallic fuel (U-Zr) with APMT cladding material and magnesium oxide (MgO) reflector. This selection was based on parameters such as a hard neutron spectrum, higher ability to reflect neutrons, low conversion factor, low leakage and an appropriate cycle length and fuel burnup. MgO reflector enabled the SACRé to operate for 6 years with a corresponding burnup of 85 MWd/KgU. Spinel ($MgAl_2O_4$) is a very competitive reflector and can be used as a substitute reflector. MgO is selected over $MgAl_2O_4$ because it provides a lower conversion ratio and leakage probability. A summary of the reactor performance characteristics per reflector material is detailed in Table 15.

Using a magnesium based reflector (Mgo or $MgAl_2O_4$) in the system promotes an easy loading configuration and the power distribution radially appears to be somewhat flat before peaking closed to the centralized reflector. Despite providing a better neutron economy, lead based reflector allow more neutron leakage and the system is further away from equilibrium. This thesis proposes nitrogen as an alternative coolant to air. Nitrogen, as presented, in this thesis will be obtained directly from air through a chemical separation process, before being introduced in the reactor. Nitrogen constitute close to 80% percent of air making it an appropriate replacement. Using nitrogen as a coolant may lead to some drawbacks with the presence of storage tanks.

6.2 **Future Work**

The primary focus of this thesis has been performing a reactor physics analysis of air as a potential coolant for a nuclear system. The system was designed and simulated with set rated power and an average coolant and fuel temperature, 575°C and 875°C respectively. These proposed assumptions are yet to be evaluated to ensure that the proposed system meet thermal needs to support its complete feasibility.

Satisfying the thermal hydraulics needs to validate the appropriateness of air to cool the reactor would require an analysis of the flow channel: inlet and outlet velocity and pressure requirements, potential adjustment of the temperature of the fuel and/or coolant, void fraction at channel exits.

This thesis proposed three different configurations and the third one was emphasized in this thesis. These configurations would need to be evaluated to determine the appropriate one; their evaluation may lead to a modification and optimization of the dimensions that will satisfy both neutronics and thermal hydraulics to ensure a complete feasibility of the system.

Table 15. SACRé System Design Summary and Performance Data.

Reflector Material	Power (MWth)	End of Cycle (Days)	End of Cycle (Years)	Burnup at EOC (MWd/KgU)		Keff	Conversion Ratio	Leakage Probability	Min Fa. Power (MWth)	Max Fa. Power (MWth)
MgO	600	2207	6	85	BOC	1.0587 +/- 0.00051	0.6309 +/- 0.023	0.0221	4.69	8.29
					EOC-1	0.9963 +/- 0.00062	0.7063 +/- 0.0025	0.0253	4.76	8.04
MgAl$_2$O$_4$		2207	6	85	BOC	1.0539 +/- 0.00059	0.6379 +/-0.0024	0.0249	4.76	8.1
					EOC-1	0.9985 +/- 0.00064	0.7108 +/-0.0025	0.0280	4.74	7.97
Al$_2$O$_3$		2207	6	85	BOC	1.0546 +/- 0.00055	0.6366 +/-0.0024	0.0237	4.80	8.09
					EOC-1	0.9989 +/- 0.00057	0.7119 +/-0.0024	0.0268	4.69	8.01
Pb		2596	7.3	100	BOC	1.03807 +/- 0.00060	0.6544 +/- 0.0025	0.0537	4.02	7.14
					EOC-4	0.9989 +/- 0.00057	0.7342 +/- 0.0026	0.0613	3.99	7.14
PbO		2596	7.1	100	BOC	1.04183 +/- 0.00056	0.6596 +/- 0.0024	0.0393	4.72	7.26
					EOC-3	0.9988 +/- 0.00062	0.7303 +/- 0.0025	0.0448	4.45	7.24
LBE		2466	6.7	95	BOC-2	1.0327 +/- 0.00066	0.6511 +/- 0.0024	0.0573	4.02	7.26
					EOC-2	0.9996 +/- 0.00067	0.7277 +/- 0.0025	0.0656	3.91	7.18

REFERENCES

[1] US Department of Energy, "Small Modular Reactor," 2015. [Online]. Available: http://www.energy.gov/ne/nuclear-reactor-technologies/small-modular-nuclear-reactors. [Accessed 20 November 2015].

[2] International Atomic Energy Agency, "Advances in Small Modular Reactor Technology Developments," International Atomic Energy Agency, 2014.

[3] M. Brudieu, "Blind Benchmark Predictions of Nacok Air Ingress Tests Using Computational Fluid Dynamics," M.I.T, 2006.

[4] N. E. Todreas and M. S. Kazimi, Nuclear Systems, 2 ed., CRC Press, 2012.

[5] N. Touran, "Fast reactors," [Online]. Available: https://whatisnuclear.com/articles/fast_reactor.html. [Accessed 20 December 2015].

[6] J. Leppannen, "Serpent-A Continuous Energy Monte Carlo Reactor Physics Burnup Calculation Code," VTT Technical Research.

[7] MATLAB, "Features," [Online]. Available: http://www.mathworks.com/products/matlab/features.html. [Accessed 20 December 2015].

[8] A. E. Waltar, A. Reynolds and P. Tsvetkov, Fast Spectrum Reactors, 2 ed., Springer, 2012.

[9] F. Carre, P. Yvon, P. Anzieu, N. Chauvin and J. Malo, "Update of the French R&D Strategy on Gas Cooled Reactors," Commissariat à l'Energie Atomique Nuclear Energy Division, 2010.

[10] Korean Atomic Energy Research Institut, "Tables of Nuclides," 2014. [Online]. Available: http://atom.kaeri.re.kr/nuchart/. [Accessed 8 August 2015].

[11] C. Sutour, C. Stumpf, J. Kosinski and A. Surget , "Determination of the Argon Concentration in Ambient Dry Air For the Calcultion of Air Density," 2007.

[12] N. Tauveron, M. Saez, M. Marchand , T. Chataing, G. Geffraye and C. Bassi, "Transient Thermal-Hydraulic Simulations of Direct Cycle Gas Cooled Reactors," 2005.

[13] P. Hejzlar, N. Todreas, E. Shwageraus, A. Nikiforova, R. Petroski and M. Driscoll, "Cross-Comparision of Fast Reactor Concepts with Various Coolant," 2009.

[14] M. McDonald, "Helium Turbomachinery Operating Experience from Gas Turbine Power Plants and Test Failities," Applied Thermal Engineering, 2012.

[15] M. Moran and H. Shapiro , Fundamentals of Engineering Thermodynamics, 5 ed., John Wiley & Sons, 2004.

[16] G. Melese-D'hopital and R. Simon, "Status of Gas-Cooled Fast Breeder Reactor Programs," Nuclear Engineering and Design, 1977.

[17] D. Lide, "CRC Handbook of Chemistry and Physics," 1997. [Online]. Available: http://www.corrosion-doctors.org/Experiments/Air.htm. [Accessed November 2015].

[18] Sandvik Group, "High Temperature Corrosion: Oxidation," [Online]. Available: http://smt.sandvik.com/en/materials-center/corrosion/high-temperature-corrosion/oxidation. [Accessed November 2015].

[19] UNSW Australia, "Material Science and Engineering: Dry Corrosion," 2013. [Online]. Available: http://www.materials.unsw.edu.au/tutorials/online-tutorials/1-dry-corrosion. [Accessed December 2015].

[20] UNSW Australia, "Material Science and Engineering: Formation of Oxide Layer," 2013. [Online]. Available: http://www.materials.unsw.edu.au/tutorials/online-tutorials/2-formation-oxide-layer. [Accessed November 2015].

[21] S. Zumdahl, Chemistry, 9 ed., Brooks & Cole Cengage Learning.

[22] B. Shleien, The Health Physics and Radiological Health Handbook, Scinta Inc., 1992.

[23] M. Ragheb, "Nuclear Reactor Concepts and Thermodynamics Cycle," 2015.

[24] E. Uckan, "Heat Exchangers Recuperators," 2015. [Online]. Available: http://www.slideshare.net/AliAbdullah18/heat-exchanger-recuperators. [Accessed 20 December 2015].

[25] Centers for Desease Control and Prevention (CDC), "Production and Atmospheric Release of Activation Products," [Online]. Available: http://www.cdc.gov/nceh/radiation/savannah/Chapter_04-3.pdf. [Accessed 20 December 2015].

[26] LENNTECH, "Chemical Properties of Argon," 2015. [Online]. Available: http://www.lenntech.com/periodic/elements/ar.htm. [Accessed 20 December 2015].

[27] Laboratoire National Henri Becquerel, "Recommended Data," 2015. [Online]. Available: http://www.nucleide.org/DDEP_WG/DDEPdata.htm. [Accessed 20 December 2015].

[28] C. Azevedo, "Selection of fuel Cladding Material for Nuclear Fission Reactors," Engineering Faillure Analysis, 2011.

[29] J. Jung , S. Kim, S. Shin, I. Bang and J. Kim, "Feasibility Study of Fuel Cladding Performace Application in Ultra-Long Cycle Fast Reactors," *Journal of Nuclear Materials,* 2013.

[30] P. Tomaszewics and G. Wallmork, "The Oxidation of High Purity Iron-Chromium-Aluminum Alloy at 800°C"," 1983.

[31] S. Chandra , S. Das and S. Maitra, "Oxidation Behavior of Silicon Carbide," 2014.

[32] Nickel Development Institut (NiDI), "High Temperature Characteristics of Stainless Steels," American Iron and Steel Institut N°9004.

[33] SandMeyer Steel Company, "Specification Sheet: Alloy 310/310S/310H".

[34] Industrial Heating, "A New High-Temperature Alloy for Extreme Temperatures," [Online]. Available: www.kanthal.com/en/products/material-datasheets/wire/na/kanthal-apmt/. [Accessed 18 December 2015].

[35] G. Green and C. Finfrock, "Oxidation of Inconel 718 in Air Temperatures from 973K to 1620K," Brookheaven National Laboratory, 2000.

[36] Ulbrich, "Inconnel 718 Datasheets," [Online]. Available: www.ulbrich.com/inconel-718/. [Accessed 18 December 2015].

[37] D. Hartanto and Y. Kim, "Alternative Reflectors for a Compact Sodium-Cooled Breed-and-Burn Fast Reactor," 2014.

[38] Skyworks Solutions Inc, "Ceramics and Advanced Materials: Magnesium Aluminate Spinel," 2014. [Online]. Available: http://www.trans-techinc.com/documents/magnesium-aluminate.pdf. [Accessed December 2015].

[39] Pacific Northwest National Laboratory, "Compendium of Material Composition for Radiation Transport Modeling," PNNL-15870 Rev.1, 2011.

[40] K. Murty and I. Charit, "Structural Materials for Gen-IV Nuclear Reactors: Challenge and Opportunities," 2008.

[41] Generation IV Roadmap, "Crosscutting Fuels and Materials R&D Scope Report," 2002.

[42] R. Klueh, J. Shingledecker, R. Swindeman and D. Hoelzer, "Oxide Dispersion-Strenghtened Steels: A Comparision of Experimental and Commercial Steel," Oak Ridge National Laboratory, 2004.

[43] R. Adams, "Nitrogen or Air Versus Helium for Nuclear Closed Cycle Gas Turbines," 2009. [Online]. Available: http://atomicinsights.com/nitrogen-or-air-versus-helium-for-nuclear-

closed-cycle-gas-turbines/. [Accessed 20 December 2015].

[44] Linde Engineering, "History and Technological Progress: Cryogenic Air Seperation".

[45] Korean Advanced Institut of Science and Technology, "Sodium Burner & Breeder Reactor," Department of Nuclear and Quantum Energy, 2013.

[46] P. Darilek and R. Zajac, "ALLEGRO-Introduction to GFR," International Atomic Energy Agency.

[47] R. Zajac and K. Michelle , "Neutronics Analysis of the European Gas-Cooled Fast Reactor Demonstrator ALLEGRO and its Validation via Monte Carlo TRIPOLI Calculations," Ecole Polytechnique De Lausanne, 2010.

[48] N. Tsoulfanidis , "Selected Entries From the Encyclopedia of Sustainability Science and Technology," Springer, 2012.

[49] F. Tingzhou, "Innovative Design of Uranium Startup Fast Reactors," Massachusetts Institute of Technology, 2012.

[50] University of Cambridge, "Material for Nuclear Power Generation: Fuel and Cladding," [Online]. Available: http://www.doitpoms.ac.uk/tlplib/nuclear_materials/fuel.php. [Accessed 20 November 2015].

[51] Encyclopedia Britannica, "Nuclear Material: Reflectors," [Online]. Available: http://www.britannica.com/technology/reflector-nuclear-reactor. [Accessed 20 December 2015].

[52] R. Vondy, "Nuclear Fuel, Mass Balances, Conversion Ratio, Doubling Time and Uncertainty," Oak Ridge National Laboratory. 3-446-0550521-8.

[53] Institut of Heat and Mass Transfer in Nuclear Power Plants , "Thermophysical Properties of MAterials for Nuclear Engineering," Kirillov, 2006.

APPENDIX

Table 16. Thermo-physical Properties of Dry Air [53].

t	ρ	C$_p$	λ	μ	a	ν	Pr
-50	1.532	1.00	2.05	14.53	13.4	9.49	0.71
-20	1.350	1.00	2.28	16.15	16.8	11.97	0.71
0	1.251	1.00	2.44	17.19	19.4	13.75	0.71
10	1.207	1.00	2.51	17.69	20.7	14.66	0.71
20	1.166	1.00	2.58	18.19	22.0	15.61	0.71
30	1.127	1.00	2.65	18.68	23.4	16.58	0.71
40	1.091	1.00	2.72	19.16	24.8	17.57	0.71
50	1.057	1.00	2.79	19.63	26.3	18.58	0.71
60	1.026	1.01	2.86	20.10	27.6	19.60	0.71
70	0.996	1.01	2.92	20.56	29.2	20.65	0.71
80	0.967	1.01	2.99	21.02	30.6	21.74	0.71
90	0.941	1.01	3.06	21.47	32.2	22.82	0.71
100	0.916	1.01	3.12	21.90	33.6	23.91	0.71
120	0.869	1.01	3.24	22.77	36.9	26.21	0.71
140	0.827	1.02	3.37	23.61	40.0	28.66	0.71
160	0.789	1.02	3.49	24.44	43.3	31.01	0.71
180	0.754	1.02	3.62	25.24	46.9	33.49	0.71
200	0.722	1.03	3.74	26.01	50.6	36.03	0.71
250	0.6530	1.03	4.06	27.91	60.0	42.75	0.71
300	0.5960	1.05	4.37	29.71	70.0	49.87	0.71
350	0.5482	1.06	4.64	31.42	80.0	57.33	0.72
100	0.5075	1.07	4.91	33.09	90.6	65.22	0.72
500	0.4418	1.09	5.45	36.15	113	81.85	0.72
600	0.3912	1.11	5.98	39.05	137	99.86	0.73
700	0.3510	1.13	6.47	41.74	162	118.95	0.73
800	0.3183	1.16	7.00	44.29	190	139.18	0.73
900	0.2916	1.17	7.40	46.68	216	160.14	0.74
1000	0.2683	1.18	7.84	48.99	247	182.67	0.74
1100	0.2487	1.20	8.26	51.20	277	205.94	0.74
1200	0.2319	1.21	8.66	53.36	309	230.17	0.74

Table 17. Chemical Composition of Cladding Materials.

Material	FeCrAl	SiC	304SS	310SS	316LSS	APMT	Inconel 718
	Weight %						
Fe	75	-	71.35	52.5	65.395	69.79	17
Cr	20	-	18.9	25.2	17	21.6	19
Al	5	-	-	-	-	4.9	0.6
Zr	-	-	-	-	-	0.1	-
Ni	-	0.5	8.35	19.5	12	-	52.5
Mn	-	-	0.7	1.9	2	-	0.35
Mo	-	-	0.27	0.13	2.5	2.8	3.05
Y	-	-	-	-	-	0.12	-
Si	-	-	0.42	0.7	1	0.53	0.35
Hf	-	-	-	-	-	0.16	-
C	-	0.5	-	-	0.03	-	0.08
Co	-	-	-	-	-	-	1
Ti	-	-	-	-	-	-	0.9
Cu	-	-	-	-	-	-	0.3
P	-	-	-	-	0.045	-	0.015
B	-	-	-	-	-	-	0.006
S	-	-	-	-	0.03	-	0.015
Nb	-	-	-	-	-	-	5.125